

Contents lists available at ScienceDirect

# Journal of the Mechanics and Physics of Solids

journal homepage: www.elsevier.com/locate/jmps





# Entropic pressure on fluctuating solid membranes

Rubayet Hassan a,1, Maria Alejandra Garzon b,1, Wei Gao b,c,\*, Fatemeh Ahmadpoor a,\*\*

- <sup>a</sup> Department of Mechanical and Industrial Engineering, New Jersey Institute of Technology, Newark, NJ 07114, United States
- <sup>b</sup> J. Mike Walker '66 Department of Mechanical Engineering, Texas A&M University, College Station, TX 77843, United States
- <sup>c</sup> Department of Materials Science and Engineering, Texas A&M University, College Station, TX 77843, United States

#### ARTICLE INFO

#### Keywords: Thermal fluctuations Entropic force Solid membranes

#### ABSTRACT

Biological and crystalline membranes exhibit noticeable fluctuations at room temperature due to their low bending stiffness. These fluctuations have a significant impact on their overall mechanical behavior and interactions with external objects. When two membranes come into proximity, they mutually suppress each other's fluctuations, leading to a repulsive force that plays a pivotal role in the mechanical behavior of these membranes. From the mechanics point of view, crystalline membranes are modeled as solid membranes with inherent shear resistance, whereas biological membranes are commonly described as fluidic entities without shear resistance. Under this premise, the entropic force between two fluctuating biological membranes is proposed to scale as  $p \propto 1/d^3$ , where d is the intermembrane distance. Yet, there are numerous instances where these membranes display shear resistance and behave akin to solid membranes. In this paper, we develop a statistical mechanics model within nonlinear elasticity to study the entropic force acting on a confined, fluctuating solid membrane. We demonstrate that, due to the nonlinear elasticity of solid membranes, the entropic force scales differently compared to that of fluid membranes. Our predictions align well with the results obtained from molecular dynamics simulations involving graphene, a representative of a solid membrane, confined between two rigid walls.

#### 1. Introduction

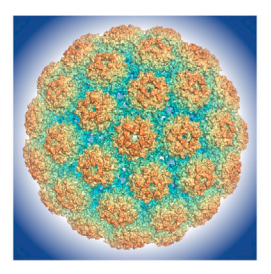
Biological and crystalline membranes fluctuate noticeably at room temperature due to their low bending stiffness. These fluctuations impact their overall mechanical response and interactions with external objects. In biology, many physiological processes are intricately linked to these thermal fluctuations. Processes such as exo and endocytosis, membrane fusion, cell adhesion, binding–unbinding transitions, the structural dynamics of red blood cell membranes, cytoskeletal interactions, and the mechanical effects induced by actin on membranes, among many others, are profoundly affected by these fluctuations (Lipowsky and Seifert, 1991; Lipowsky and Leibler, 1986; Lee et al., 2010; Weikl and Lipowsky, 2004; Chen et al., 2008; Gao et al., 2005; Ahmadpoor and Sharma, 2016,b; Gov et al., 2003; Dearnley et al., 2016; Kusters et al., 2019). Consequently, the exploration of entropic factors in biological phenomena has evolved into a cornerstone of cell mechanics research (Kulkarni, 2023; Fisher, 1993; Lee et al., 2010; Weikl and Lipowsky, 2004; Chen et al., 2008; Lipowsky and Leibler, 1986; Farago and Santangelo, 2005; Auth et al., 2007; Helfrich, 1986; Ahmadpoor and Sharma, 2016b; Huang et al., 2017; Freund, 2013; Sharma, 2013; Zelisko et al., 2017). The biophysical processes mentioned above are orchestrated by a sophisticated interplay between a set of attractive and repulsive forces that

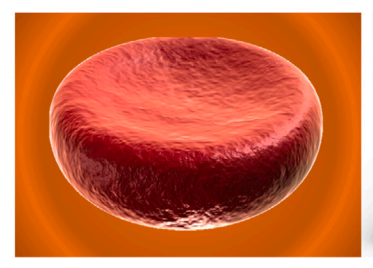
<sup>\*</sup> Correspondence to: J. Mike Walker '66 Department of Mechanical Engineering, 3123 TAMU, College Station, TX 77843-3123, United States

<sup>\*\*</sup> Corresponding author.

E-mail addresses: wei.gao@tamu.edu (W. Gao), fatemeh.ahmadpoor@njit.edu (F. Ahmadpoor).

<sup>&</sup>lt;sup>1</sup> Equal contributions.





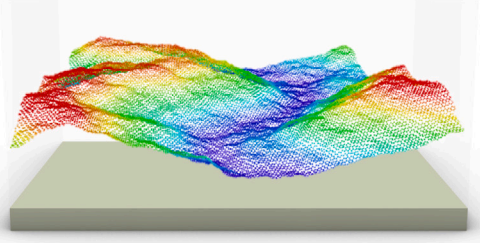


Fig. 1. Solid membranes are ubiquitous. Examples include viral capsid (the left), red blood cell membranes (the middle), and crystalline membranes such as graphene (the right).

mediate between biological structures. Central to this interplay is a repulsive force known as *entropic pressure*, originating from the thermally induced fluctuations in membranes. When an external object approaches a fluctuating membrane, it impedes the membrane's out-of-plane fluctuations. This interference results in a reduction of system entropy that varies with the distance between the membrane and the obstructing object. As a result, a repulsive force is generated, which acts to separate the membrane from the external object. The same behavior appears when a crystalline membrane is placed on a substrate (Wang et al., 2016) or in contact with another membrane (Zhu et al., 2022). Such entropic pressure was first addressed in the context of cell-cell interactions by Helfrich (1978) and subsequently examined by several groups in both physics (Bachmann et al., 2001; Kleinert, 1999) and mechanics communities (Freund, 2013; Sharma, 2013; Hanlumyuang et al., 2014; Liang and Purohit, 2018; Mozaffari et al., 2021). From the mechanics point of view, the fluctuating membrane is modeled as a fluid elastic sheet with bending deformations and no shear resistance. Based on this assumption, Helfrich (1978) proposed that entropic force between two fluctuating membranes in distance d should scale as  $p \propto 1/d^3$ . This power law has been later verified in other theoretical and computational models (Bachmann et al., 2001; Kleinert, 1999; Hanlumyuang et al., 2014; Ahmadpoor et al., 2019, 2022).

Although biological membranes are commonly modeled as fluid membranes, there are instances where they possess an *apparent* shear resistance—some examples are demonstrated in Fig. 1. One such example can be found in the membranes of red blood cells (RBCs), which endure consistent mechanical stresses within the bloodstream. Despite the continuous exposure to flow and the substantial deformations they undergo when squeezed through narrow capillaries (Noguchi and Gompper, 2005), the lifespan of RBCs surpasses that of artificial vesicles designed for drug delivery by several orders of magnitude (Lasic, 1994). A pivotal factor in maintaining the structural integrity of RBCs is the presence of a network composed of flexible spectrin polymers, forming a two-dimensional cytoskeleton, which imparts shear resistance to the membrane. The spectrin cytoskeleton is typically modeled as a solid membrane. Another example is viral capsid shells. The study of the mechanical behavior of capsids is of particular interest to the biomechanics and mechanobiology community for understanding the morphology of viruses that impact their interactions with their surrounding bioenvironment. Besides biological examples, crystalline membranes such as graphene, boron nitride, MXene among many others are also modeled as solid membranes. These membranes may encounter noticeable entropic forces, particularly when placed on a substrate or interacting with another membrane (Wang et al., 2016; Ahmadpoor et al., 2022). Further, such entropic forces appeared to have implications for crystalline interfaces as well (Chen and Kulkarni, 2015, 2017, 2013; Zhu et al., 2022).

The elasticity of solid membranes presents a more challenging scenario when compared to their fluid counterparts. Unlike fluid membranes, solid membranes can feature not only bending and stretching rigidities but also non-trivial in-plane shear deformations that nonlinearly interact with the out-of-plane displacement field. To characterize the elasticity of solid membranes, the von Karman nonlinear plate theory is commonly employed. Studying the statistical mechanics of solid membranes is intricate due to the necessity for accounting for nonlinear geometric deformations. The majority of approaches in the literature heavily rely on analogies from the high-energy physics realm and prove challenging to adapt to the common contexts of mechanics. Recently, Ahmadpoor et al. (2017) presented a *mechanics-based* approach for dealing with nonlinearities and studied the thermal fluctuations of a free-standing solid membrane. Specifically, they introduced a variational approximation method that is closely linked to principles well-known within the mechanics community. Using this approach (Ahmadpoor et al., 2017) explored the size and temperature dependency of the out-of-plane fluctuations, and demonstrated how an elastic sheet becomes effectively stiffer at larger sizes. Nonetheless, the influence of these nonlinearities on the entropic forces exerted on a confined solid membrane has yet to be investigated.

In this paper, we formulate the entropic force on a confined fluctuating solid membrane. To deal with geometric nonlinearities, we rely on the approximate method developed by Ahmadpoor et al. (2017) to establish the scaling law for the entropic force within nonlinear elasticity. In order to reconcile our analytical results with atomistic considerations, we conduct molecular dynamics simulations using graphene as a representative solid membrane. In Section 2, we briefly review the nonlinear elasticity of the solid membranes. Setup of the statistical mechanics problem, for a confined nonlinear elastic sheet is presented in Section 3. Analytical approximate solutions are derived for the entropic force using the variational perturbation method in Section 4. Detailed descriptions of the molecular dynamics simulations and their outcomes can be found in Section 5. Finally, our findings will be summarized in Section 6.

#### 2. Review of the nonlinear elasticity of the solid membranes

Let us consider a flat, elastic sheet that lies in the x-y plane, with dimensions given by a square domain of size  $S = (0, L)^2$ . Initially, at zero Kelvin which represents the undeformed ground state the sheet is placed on the z=0 plane. To specify any point on the surface S, we can use its position vector, denoted as x. We then, introduce a vector field u defined on the surface S, which represents the displacement field of the sheet. Consequently, the position of each point on the deformed surface can be expressed as  $\mathbf{r} = \mathbf{x} + \mathbf{u}$ . The displacement field using Monge parametrization can be expressed as:

$$\mathbf{u} = (u_x, u_y, h),\tag{1}$$

where  $u_x$  and  $u_y$  are displacement fields along x and y directions, respectively and h is the out-of-plane displacement field. Then the in-plane strain field is defined as:

$$\mathcal{E}_{\gamma\delta} = \frac{1}{2} \left( \frac{\partial u_{\gamma}}{\partial x_{\delta}} + \frac{\partial u_{\delta}}{\partial x_{\gamma}} + \frac{\partial h}{\partial x_{\gamma}} \frac{\partial h}{\partial x_{\delta}} \right). \tag{2}$$

The resulting stress tensor, assuming isotropy, can be written as:

$$\sigma_{\gamma\delta} = \frac{E}{1 - v^2} \left( \mathcal{E}_{\gamma\delta} + \frac{v}{1 - v} \mathcal{E}_{kk} \delta_{\gamma\delta} \right),\tag{3}$$

where E and v are the elastic Young modulus and Poisson ratio of the solid sheet, respectively. The in-plane stretching energy can then be expressed as:

$$U_s = \int_{\mathcal{S}} \frac{1}{2} \sigma_{\gamma \delta} \mathcal{E}_{\gamma \delta} = \int_{\mathcal{S}} U_I + U_{II} + U_{III}, \tag{4}$$

in which,

$$U_{I} = \frac{E}{2(1 - v^{2})} \left( \left( \frac{\partial u_{x}}{\partial x} \right)^{2} + \left( \frac{\partial u_{y}}{\partial y} \right)^{2} + 2v \frac{\partial u_{x}}{\partial x} \frac{\partial u_{y}}{\partial y} \right) + \frac{E}{4(1 + v)} \left( \frac{\partial u_{x}}{\partial y} + \frac{\partial u_{y}}{\partial x} \right)^{2}, \tag{5a}$$

$$U_{II} = \frac{E}{2(1 - v^2)} \left( \frac{\partial u_x}{\partial x} \left( \frac{\partial h}{\partial x} \right)^2 + \frac{\partial u_y}{\partial y} \left( \frac{\partial h}{\partial y} \right)^2 + v \frac{\partial u_x}{\partial x} \left( \frac{\partial h}{\partial y} \right)^2 + v \frac{\partial u_y}{\partial y} \left( \frac{\partial h}{\partial x} \right)^2 \right)$$

$$+\frac{E}{2(1-v^2)}\frac{\partial h}{\partial x}\frac{\partial h}{\partial y}\left(\frac{\partial u_x}{\partial y} + \frac{\partial u_y}{\partial x}\right),\tag{5b}$$

$$U_{III} = \frac{E}{8(1+\nu)} \left( \left( \frac{\partial h}{\partial x} \right)^4 + \left( \frac{\partial h}{\partial y} \right)^4 + 2 \left( \frac{\partial h}{\partial x} \frac{\partial h}{\partial y} \right)^2 \right) = \frac{E}{8(1-\nu^2)} |\nabla h|^4.$$
 (5c)

In addition, the out-of-plane displacement field creates curvature and bending deformations on the surface. Let  $c_1$  and  $c_2$  be the principal curvatures<sup>2</sup> at each point on the surface. Then the mean and Gaussian curvatures are obtained as (Abbena et al., 2006):

$$H = \frac{1}{2}(c_1 + c_2), \qquad K = c_1 c_2. \tag{6}$$

Up to quadratic order, the bending energy associated with the curvature field is given as (Zhong-Can and Helfrich, 1989):

$$U_b = \int_{\mathcal{C}} \frac{1}{2} \kappa_b (c_1 + c_2)^2 + \kappa_G c_1 c_2, \tag{7}$$

where,  $\kappa_b$  and  $\kappa_G$  are the bending and Gaussian moduli, respectively. Further, due to the Gauss–Bonnet theorem (Abbena et al., 2006), the integration of Gaussian curvature over a 2D *closed* area is fixed when the topology of the system does not change in the deformed configuration. Thus, in what follows, we disregard the second term in Eq. (7). As long as the deviations from the flat state are small ( $|\nabla h| \ll 1$ ), the linearized mean curvature (H) may be used and is described in terms of the out-of-plane displacement as follows:

$$2H = c_1 + c_2 = \frac{\partial^2 h}{\partial x^2} + \frac{\partial^2 h}{\partial y^2} = \nabla^2 h. \tag{8}$$

The total energy can then be described as the summation of the bending and stretching energy terms,  $U = U_b + U_S$ . This total energy will be out starting point for setting up the statistical mechanics problem of a confined solid membrane in Section 3.

# 3. Setup of the statistical mechanics problem

The elastic energy cost to deform a planar solid membrane is given by:  $U = U_b + U_s$ . When the temperature is at absolute zero (T = 0 Kelvin), and no external forces are present, the membrane naturally tends to maintain its flat shape to minimize its

<sup>&</sup>lt;sup>2</sup> Curvatures at a point can be evaluated in any direction but have a maximum and minimum values along two particular orthogonal directions. The corresponding maximum and minimum values of the curvature at a given point are referred to as the principal curvatures.

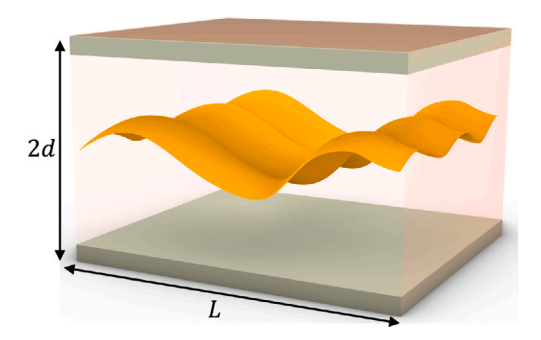


Fig. 2. Schematic of a fluctuating solid membrane of size  $L^2$ , confined within two hard walls in distance 2d.

overall elastic energy. However, when the temperature is above zero, the sheet undergoes dynamic fluctuations and experiences non-flat configurations that involve both in-plane and out-of-plane deformations. Each of these modes is associated with a probability distribution that is described by Boltzmann factor (Kittel, 2004):

$$\rho_i \propto \exp(-U_i/k_BT)$$
,

where  $k_BT$  is the thermal energy,  $\rho_i$  is the probability of occurrence of mode i and  $U_i$  is its associated energy. The probability distribution can be normalized to 1 through the normalizing factor 1/Z, where Z is the so-called partition function and is obtained by summing over all possible configurations (Kittel, 2004) which in this continuous system are uncountably infinite:

$$Z = \sum_i \exp(-U_i/k_BT).$$

The probability distribution allows the computation of the ensemble average of any physical quantity  $\mathcal{X}$  that is obtained as (Kittel, 2004):

$$\langle \mathcal{X} \rangle = \frac{1}{Z} \sum_i \mathcal{X}_i \text{exp}(-U_i/k_B T).$$

Now consider a fluctuating solid membrane confined within two hard walls in distance 2d from one another as shown in Fig. 2, such that the fluctuations are limited to -d < h < d. We assume periodic boundary conditions in all directions to ensure in-plane translational and rotational symmetry. For this case the partition function and the free energy are expressed as functions of d:

$$Z[d] = \int_{-\infty}^{\infty} \int_{-d}^{d} \exp\left(-\frac{U_b + U_S}{k_B T}\right) \mathcal{D}[\mathbf{u}, h], \qquad F[d] = -k_B T \log Z. \tag{9}$$

The entropic pressure is then calculated by taking the derivative of the free energy with respect to the volume V:

$$p = -\frac{\partial F}{\partial V} = -\frac{1}{2L^2} \frac{\partial F}{\partial d}.$$

The partition function in Eq. (9) cannot be carried out analytically, because:

- 1. the confinement on the fluctuations leads to the finite integral bounds (-d,d) for the out-of-plane displacement h; and
- 2. the energy function in the exponent is anharmonic with respect to the out-of-plane displacement h.

To remedy the first issue, following the past theoretical models of entropic force on fluctuating membranes (Helfrich, 1978; Mozaffari et al., 2021; Ahmadpoor et al., 2022), we introduce a potential energy term added to the original elastic energy to *mimic* the effects of the entropic pressure on the suppression of fluctuations and instead, carry out the partition function integration within  $(-\infty, \infty)$ . We then *tune* the potential energy in such a way that:  $\langle h^2 \rangle < d^2$ . Now let

$$U^{\text{tot}} = U_b + U_S + U_P [h] \tag{10}$$

be the total energy, including the potential energy  $U_P[h]$ . In general,  $U_P[h]$  can be expanded in a polynomial form as:

$$U_P[h] = \int \alpha_2 h^2 + \alpha_4 h^4 + \alpha_6 h^6 + \cdots$$

The potential energy  $U_P[h]$  ensures a lower probability for larger values of h and, eventually, decreases the fluctuations. To facilitate analytical derivation, we keep only the quadratic term in  $U_P[h]$ . Thus, the total energy can be written as:

$$U^{\text{tot}} = \int \left[ \frac{1}{2} \kappa_b (\nabla^2 h)^2 + \frac{1}{2} \gamma_d h^2 + U_I + U_{III} + U_{III} \right] dS, \tag{11}$$

where  $\gamma_d$  is a *tuning* parameter that depends on d and ensures lower probability for larger fluctuations, such that  $\langle h^2 \rangle < d^2$ . The new partition function is then obtained as:

$$Z = \int_{-\infty}^{\infty} \int_{-\infty}^{\infty} \exp\left(-\frac{1}{k_B T} \int \left[\frac{1}{2} \kappa_b (\nabla^2 h)^2 + \frac{1}{2} \gamma_d h^2 + U_I + U_{III} + U_{III}\right] dS\right) \mathcal{D}\left[\mathbf{u}, h\right]. \tag{12}$$

The partition function in (12) resolves the issue with the integral bounds. We now return our attention to the second issue associated with geometric nonlinearities and the coupling between in and out-of-plane displacement fields in the last two terms of the energy (11);  $U_{II}+U_{III}$ . The total elastic energy in (11) is anharmonic with respect to h but harmonic in terms of h. The partition function integration cannot be easily handled over h, but may be evaluated with respect to h. To start, one needs to discretize the displacement fields in Fourier space:

$$\mathbf{u}(\mathbf{x}) = \sum_{\mathbf{q} \in \mathcal{K}} \overline{\mathbf{u}}(\mathbf{q}) e^{i\mathbf{q} \cdot \mathbf{x}},\tag{13a}$$

$$h(\mathbf{x}) = \sum_{\mathbf{q} \in \mathcal{C}} \overline{h}(\mathbf{q}) e^{i\mathbf{q} \cdot \mathbf{x}},\tag{13b}$$

$$\frac{\partial h(\mathbf{x})}{\partial x_{\gamma}} \frac{\partial h(\mathbf{x})}{\partial x_{\delta}} = \sum_{\mathbf{q} \in \mathcal{K}} \overline{A}_{\gamma \delta}(\mathbf{q}) \mathbf{e}^{i\mathbf{q} \cdot \mathbf{x}},\tag{13c}$$

where  $\mathcal{K} := \{\mathbf{q} = 2\pi(v_x, v_y)/L : v_x, v_y \in \mathbb{Z}, |\mathbf{q}| \geqslant 2\pi/L\}$  and  $\gamma, \delta$  denote x, y. The Fourier transforms of the displacement fields are:

$$\overline{\mathbf{u}}(\mathbf{q}) = \frac{1}{L^2} \int_{\mathbb{S}} \mathbf{u}(\mathbf{x}) \mathbf{e}^{-i\mathbf{q}\cdot\mathbf{x}} d\mathbf{x},\tag{14a}$$

$$\overline{h}(\mathbf{q}) = \frac{1}{L^2} \int_{\mathbb{S}} h(\mathbf{x}) e^{-i\mathbf{q} \cdot \mathbf{x}} d\mathbf{x}, \tag{14b}$$

$$\overline{A}_{\gamma\delta}(\mathbf{q}) = \frac{1}{L^2} \int_{\mathbb{S}} \frac{\partial h(\mathbf{x})}{\partial x_{\gamma}} \frac{\partial h(\mathbf{x})}{\partial x_{\delta}} e^{-i\mathbf{q}\cdot\mathbf{x}} d\mathbf{x}. \tag{14c}$$

Substituting the Fourier expansions in the expression for the total energy in (11) yields the following:

$$U^{\text{tot}} = \frac{L^2}{2} \sum_{\mathbf{q} \in \mathcal{K}} \left( (\kappa_b |\mathbf{q}|^4 + \gamma_d) |\overline{h}(\mathbf{q})|^2 + \overline{U}_I(\mathbf{q}) + \overline{U}_{III}(\mathbf{q}) + \overline{U}_{III}(\mathbf{q}) \right), \tag{15}$$

where

$$\overline{U}_{I}(\mathbf{q}) = \frac{E}{1 - v^{2}} \left( \mathbf{q}^{2} |\overline{\mathbf{u}}(\mathbf{q})|^{2} + 2vq_{x}\overline{u}_{x}(\mathbf{q})q_{y}\overline{u}_{y}(\mathbf{q}) \right) 
+ \frac{E}{1 + v} \left( q_{y}^{2} |\overline{u}_{x}(\mathbf{q})|^{2} + q_{x}^{2} |\overline{u}_{y}(\mathbf{q})|^{2} - 2q_{x}q_{y}\overline{u}_{x}(\mathbf{q})\overline{u}_{y}(-\mathbf{q}) \right),$$
(16a)

$$\overline{U}_{II}(\mathbf{q}) = \frac{E}{1 - v^2} \left\{ \overline{A}_{xx}^{\text{Re}}(\mathbf{q}) (q_x \overline{u}_x^{\text{Im}}(\mathbf{q}) + v q_y \overline{u}_y^{\text{Im}}(\mathbf{q})) + \overline{A}_{yy}^{\text{Re}}(\mathbf{q}) (q_y \overline{u}_y^{\text{Im}}(\mathbf{q}) + v q_x \overline{u}_x^{\text{Im}}(\mathbf{q})) - \overline{A}_{xx}^{\text{Im}}(\mathbf{q}) (q_y \overline{u}_x^{\text{Re}}(\mathbf{q}) + v q_x \overline{u}_x^{\text{Re}}(\mathbf{q})) - \overline{A}_{yy}^{\text{Im}}(\mathbf{q}) (q_y \overline{u}_y^{\text{Re}}(\mathbf{q}) + v q_x \overline{u}_x^{\text{Re}}(\mathbf{q})) \right\} 
+ \frac{E}{1 + v} \left\{ \overline{A}_{xy}^{\text{Re}}(\mathbf{q}) (q_y \overline{u}_x^{\text{Im}}(\mathbf{q}) + q_x \overline{u}_y^{\text{Im}}(\mathbf{q})) - \overline{A}_{xy}^{\text{Im}}(\mathbf{q}) (q_y \overline{u}_x^{\text{Re}}(\mathbf{q}) + q_x \overline{u}_y^{\text{Re}}(\mathbf{q})) \right\}, \tag{16b}$$

$$\overline{U}_{III}(\mathbf{q}) = \frac{E}{4(1-v^2)} \left( \left| \overline{A}_{xx}(\mathbf{q}) \right|^2 + \left| \overline{A}_{yy}(\mathbf{q}) \right|^2 + 2\left| \overline{A}_{xy}(\mathbf{q}) \right|^2 \right). \tag{16c}$$

In the expression for  $\overline{U}_{II}(\mathbf{q})$ , the superscripts "Re" and "Im" stand for the real and imaginary parts of the Fourier transforms. For details of the derivations, the reader is referred to Appendix A. We now proceed to plug the total energy in Fourier space presented in (15) into the partition function and carry out the path integral over the in-plane displacement field:

$$Z = \int \exp(-U^{\text{tot}}/k_B T) \mathcal{D}[h, \mathbf{u}]$$

$$= \prod_{\mathbf{q} \in \mathcal{K}} \int_{-\infty}^{\infty} \exp\left(-\frac{L^2}{2k_B T} \left( (\kappa_b |\mathbf{q}|^4 + \gamma_d) |\overline{h}(\mathbf{q})|^2 + \overline{U}_I(\mathbf{q}) + \overline{U}_{II}(\mathbf{q}) + \overline{U}_{III}(\mathbf{q}) \right) \right) d\overline{h}(\mathbf{q}) d\overline{\mathbf{u}}(\mathbf{q})$$

$$= \prod_{\mathbf{q} \in \mathcal{K}} \int \alpha(\nu) \left( \frac{2\pi k_B T}{EL^2 |\mathbf{q}|^2} \right)^2 \exp\left(-\frac{L^2}{2k_B T} \left( (\kappa_b |\mathbf{q}|^4 + \gamma_d) |\overline{h}(\mathbf{q})|^2 + \overline{U}_{\text{eff}}(\mathbf{q}) \right) \right) d\overline{h}(\mathbf{q}), \tag{17}$$

where  $\alpha(v) = 1 + v - v^2 - v^3$ . As a result, the remaining terms in the exponent can be expressed in terms of an <u>effective strain energy</u>,  $\overline{U}_{eff}(\mathbf{q})$ , which is solely a function of the out-of-plane displacement and can be written as:

$$\overline{U}_{\text{eff}}(\mathbf{q}) = \frac{1}{4} E |P_{ij}^T(\mathbf{q}) \overline{A}_{ij}(\mathbf{q})|^2, \tag{18}$$

<sup>&</sup>lt;sup>3</sup> For details of these derivations the reader is referred to the Appendix B as well as (Ahmadpoor et al., 2017).

in which

$$P_{ij}^T(\mathbf{q}) = \delta_{ij} - \frac{q_i q_j}{\mathbf{q}^2}.$$
 (19)

Up to this point, we have decoupled the in and out-of-plane displacement fields and are left with a new form of energy that is merely a function of the out-of-plane displacement field. The new energy form is as follows:

$$U = \frac{1}{2}L^2 \sum_{\mathbf{q} \in \mathcal{F}} \left( (\kappa_b |\mathbf{q}|^4 + \gamma_d) |\overline{h}(\mathbf{q})|^2 + \frac{1}{4} E |P_{ij}^T(\mathbf{q}) \overline{A}_{ij}(\mathbf{q})|^2 \right). \tag{20}$$

This new energy form will be used to study the statistical mechanics of a confined fluctuating solid membrane.

### 4. Entropic force on a fluctuating solid membrane

In this section, we study the fluctuations of the out-of-plane displacement field, the free energy, and the entropic force for a confined solid membrane. We will use the nonlinear energy function in Eq. (20) as the starting point. As mentioned before, dealing with nonlinearities in statistical mechanics problems of membranes is quite challenging, and closed-form analytical solutions are frequently unachievable. Here, we will use the variational perturbation theory (VPT) to get approximate solutions for fluctuations and free energy. The central idea of the VPT was first introduced by Kleinert (2009) in the context of anharmonic Hamiltonians in quantum mechanics and later on implemented in a mechanics-based framework by Ahmadpoor and Sharma (2016b), Ahmadpoor et al. (2017), Mozaffari et al. (2021). The idea is that the effects of nonlinearities can be embedded in a so-called *renormalized* quadratic energy, that can be then used in the equipartition theorem. In the past this method has been successfully employed in the context of nonlinear elasticity of continuum systems (Ahmadpoor et al., 2015; Ahmadpoor and Sharma, 2016b; Ahmadpoor et al., 2017; Mozaffari et al., 2021).

To apply VPT we start with a trial quadratic energy function as follows:

$$U_{trial} = \frac{1}{2} L^2 \sum_{\mathbf{k} \in \mathcal{K}} \left[ \kappa^{\text{eff}}(\mathbf{k}) |\mathbf{k}|^4 + \gamma_d \right] \left| \overline{h}(\mathbf{k}) \right|^2, \tag{21}$$

where  $\kappa^{\text{eff}}(\mathbf{k})$  is the unknown effective stiffness in general mode-dependent form. Based on this trial energy, the ensemble average of the fluctuations can be obtained by equipartition theorem as:

$$\langle \left| \overline{h}(\mathbf{k}) \right|^2 \rangle = \frac{k_B T}{L^2(\kappa^{\text{eff}}(\mathbf{k})|\mathbf{k}|^4 + \gamma_d)}.$$
 (22)

Further, the variational free energy up to the Mth order is expanded in Taylor series as:

$$F_{M} = F_{0} - k_{B}T \sum_{N=1}^{M} \frac{(-1)^{N}}{(k_{B}T)^{N}N!} \langle (U - U_{trial})^{N} \rangle_{U_{trial}}^{c}, \tag{23}$$

where  $F_0$  is the free energy associated with the trial energy  $U_{trial}$  in (21):

$$F_0 = C_F + \sum_{\mathbf{k} \in \mathcal{K}} \frac{1}{2} k_B T \log \left( \frac{\kappa^{\text{eff}}(\mathbf{k}) |\mathbf{k}|^4 + \gamma_d}{k_B T} \right), \tag{24}$$

in which  $C_F$ , is a constant of no consequences. To get an optimized approximation of the free energy, we proceed to minimize the sensitivity of the series in (23) to the trial energy function,  $U_{trial}$ :

$$\frac{\partial F_M}{\partial \kappa^{\text{eff}}(\mathbf{k})} := 0. \tag{25}$$

We now proceed to expand the variational free energy in (23) up to the first order. Details of the derivations are explained in Appendix C. Up to the first order, the variational free energy is obtained as:

$$F_{var} = C_F + \sum_{\mathbf{k} \in \mathcal{K}} \left[ \frac{1}{2} k_B T \log \left( \frac{\kappa^{\text{eff}}(\mathbf{k}) |\mathbf{k}|^4 + \gamma_d}{k_B T} \right) + \frac{1}{2} k_B T \frac{(\kappa_b |\mathbf{k}|^4 + \gamma_d)}{(\kappa^{\text{eff}}(\mathbf{k}) |\mathbf{k}|^4 + \gamma_d)} \right. \\ \left. + E \sum_{\mathbf{q} \in \mathcal{K}} \frac{(k_B T)^2 |\mathbf{k}|^4 (\sin \theta_{\mathbf{q}, \mathbf{k}})^4}{8L^2 (\kappa^{\text{eff}}(\mathbf{k}) |\mathbf{k}|^4 + \gamma_d) (\kappa^{\text{eff}}(\mathbf{q} - \mathbf{k}) |\mathbf{q} - \mathbf{k}|^4 + \gamma_d)} \right],$$

$$(26)$$

where,  $\theta_{q,k}$  is the angle between the vectors  $\mathbf{q}$  and  $\mathbf{k}$ . In order to minimize the sensitivity of the variational free energy with respect to  $U_{trial}$ , we set:

$$\frac{\partial F_{var}}{\partial \kappa^{\text{eff}}(\mathbf{k})} := 0$$

$$0 := \frac{k_B T |\mathbf{k}|^4}{2(\kappa^{\text{eff}}(\mathbf{k})|\mathbf{k}|^4 + \gamma_d)} - \frac{k_B T (\kappa_b |\mathbf{k}|^4 + \gamma_d) |\mathbf{k}|^4}{2(\kappa^{\text{eff}}(\mathbf{k})|\mathbf{k}|^4 + \gamma_d)^2}$$

$$- E \sum_{\mathbf{q} \in \mathcal{K}} \frac{(k_B T)^2 |\mathbf{k}|^4 (\sin \theta_{\mathbf{q}, \mathbf{k}})^4}{8L^2 (\kappa^{\text{eff}}(\mathbf{k})|\mathbf{k}|^4 + \gamma_d) (\kappa^{\text{eff}}(\mathbf{q} - \mathbf{k}) |\mathbf{q} - \mathbf{k}|^4 + \gamma_d)} \times \left( \frac{|\mathbf{k}|^4}{\kappa^{\text{eff}}(\mathbf{k})|\mathbf{k}|^4 + \gamma_d} + \frac{|\mathbf{q} - \mathbf{k}|^4}{\kappa^{\text{eff}}(\mathbf{q} - \mathbf{k}) |\mathbf{q} - \mathbf{k}|^4 + \gamma_d} \frac{\partial \kappa^{\text{eff}}(\mathbf{q} - \mathbf{k})}{\partial \kappa^{\text{eff}}(\mathbf{k})} \right). \tag{27}$$

Assuming that at long wave-length fluctuations the effective bending stiffness  $\kappa_{\rm eff}(\mathbf{k})$ , scales as:  $\kappa_{\rm eff}(\mathbf{k}) \sim |\mathbf{k}|^{-\zeta}$  (Nelson and Peliti, 1987; Ahmadpoor et al., 2017), we have<sup>4</sup>:

$$\frac{\partial \kappa^{\text{eff}}(\mathbf{q} - \mathbf{k})}{\partial \kappa^{\text{eff}}(\mathbf{k})} = \frac{\partial \kappa^{\text{eff}}(\mathbf{q} - \mathbf{k})/\partial \mathbf{k}}{\partial \kappa^{\text{eff}}(\mathbf{k})/\partial \mathbf{k}} = \frac{|\mathbf{q} - \mathbf{k}|^{-\zeta - 1}}{|\mathbf{k}|^{-\zeta - 1}} = \frac{\kappa^{\text{eff}}(\mathbf{q} - \mathbf{k})}{\kappa^{\text{eff}}(\mathbf{k})} \frac{|\mathbf{k}|}{|\mathbf{q} - \mathbf{k}|}.$$
(28)

Substituting Eq. (28) into (27), we obtain:

$$\frac{\partial F_{var}}{\partial \kappa^{\text{eff}}(\mathbf{k})} = \frac{k_B T |\mathbf{k}|^4}{2(\kappa^{\text{eff}}(\mathbf{k})|\mathbf{k}|^4 + \gamma_d)} - \frac{k_B T (\kappa_b |\mathbf{k}|^4 + \gamma_d)|\mathbf{k}|^4}{2(\kappa^{\text{eff}}(\mathbf{k})|\mathbf{k}|^4 + \gamma_d)^2} \\
-E \sum_{\mathbf{q} \in \mathcal{K}} \frac{(k_B T)^2 |\mathbf{k}|^4 (\sin \theta_{\mathbf{q},\mathbf{k}})^4}{8L^2 (\kappa^{\text{eff}}(\mathbf{k})|\mathbf{k}|^4 + \gamma_d)(\kappa^{\text{eff}}(\mathbf{q} - \mathbf{k})|\mathbf{q} - \mathbf{k}|^4 + \gamma_d)} \\
\times \left( \frac{|\mathbf{k}|^4}{\kappa^{\text{eff}}(\mathbf{k})|\mathbf{k}|^4 + \gamma_d} + \frac{|\mathbf{q} - \mathbf{k}|^3 |\mathbf{k}|}{\kappa^{\text{eff}}(\mathbf{q} - \mathbf{k})|\mathbf{q} - \mathbf{k}|^4 + \gamma_d} \frac{\kappa^{\text{eff}}(\mathbf{q} - \mathbf{k})}{\kappa^{\text{eff}}(\mathbf{k})} \right) = 0.$$
(29)

Solving Eq. (29) for  $\kappa^{\text{eff}}(\mathbf{k})$ , we obtain the following implicit equation:

$$\kappa^{\text{eff}}(\mathbf{k}) = \kappa_b + \frac{k_B T E}{4L^2} \sum_{\mathbf{q} \in \mathcal{K}} \left( \frac{\kappa^{\text{eff}}(\mathbf{q} - \mathbf{k}) \left(\kappa^{\text{eff}}(\mathbf{k}) |\mathbf{k}|^4 + \gamma_d\right) \left(\sin \theta_{\mathbf{q}, \mathbf{k}}\right)^4}{\kappa^{\text{eff}}(\mathbf{k}) \left(\kappa^{\text{eff}}(\mathbf{q} - \mathbf{k}) |\mathbf{q} - \mathbf{k}|^4 + \gamma_d\right)^2} \left| \frac{\mathbf{q} - \mathbf{k}}{\mathbf{k}} \right|^3 + \frac{\left(\sin \theta_{\mathbf{q}, \mathbf{k}}\right)^4}{\kappa^{\text{eff}}(\mathbf{q} - \mathbf{k}) |\mathbf{q} - \mathbf{k}|^4 + \gamma_d} \right). \tag{30}$$

The first step to solve the implicit equation in (30) is to carry out the summation in the second and third terms over  $\mathbf{q}$ . Following the scaling analysis presented in Ahmadpoor et al. (2017), we set  $\kappa^{\mathrm{eff}}(\mathbf{q} - \mathbf{k}) \sim \Theta |\mathbf{q} - \mathbf{k}|^{-\zeta}$ , with  $\Theta$  representing an unknown constant. In order to make analytical progress, we consider two cases:

- 1. Large intermembrane distance: In this case, the fluctuations, although confined and suppressed by the entropic force, are large enough to generate in-plane nonlinear strain energy. Thus,  $\gamma_d$  will be quite small and negligible compared to the nonlinear effect of the in-plane strain energy.
- 2. Small intermembrane distance: In this case, the entropic force will suppress both the fluctuations and the resulting nonlinear in-plane strain. For this case,  $\gamma_d$  will be indeed dominant and cannot be neglected.

We start with the first case, where the distance d is large and  $\gamma_d$  is quite small and negligible. The summation in (30) for this case, scales as:

$$\frac{1}{L^{2}} \sum_{\mathbf{q} \in \mathcal{K}} \left( \frac{\kappa^{\text{eff}}(\mathbf{q} - \mathbf{k}) \left( \kappa^{\text{eff}}(\mathbf{k}) |\mathbf{k}|^{4} + \gamma_{d} \right) \left( \sin \theta_{\mathbf{q}, \mathbf{k}} \right)^{4}}{\kappa^{\text{eff}}(\mathbf{k}) \left( \kappa^{\text{eff}}(\mathbf{q} - \mathbf{k}) |\mathbf{q} - \mathbf{k}|^{4} + \gamma_{d} \right)^{2}} \left| \frac{\mathbf{q} - \mathbf{k}}{\mathbf{k}} \right|^{3} + \frac{\left( \sin \theta_{\mathbf{q}, \mathbf{k}} \right)^{4}}{\kappa^{\text{eff}}(\mathbf{q} - \mathbf{k}) |\mathbf{q} - \mathbf{k}|^{4} + \gamma_{d}} \right) 
\sim \frac{1}{L^{2}} \sum_{\mathbf{q} \in \mathcal{K}} \frac{\left( \sin \theta_{\mathbf{q}, \mathbf{k}} \right)^{4}}{\kappa^{\text{eff}}(\mathbf{q} - \mathbf{k}) |\mathbf{q} - \mathbf{k}|^{4}} \left( 1 + \frac{|\mathbf{k}|}{|\mathbf{q} - \mathbf{k}|} \right) + O(\gamma_{d}) 
\sim \frac{1}{L^{2}} \sum_{\mathbf{q} \in \mathcal{K}} \frac{\left( \sin \theta_{\mathbf{q}, \mathbf{k}} \right)^{4}}{\Theta |\mathbf{q} - \mathbf{k}|^{4 - \eta}} \left( 1 + \frac{|\mathbf{k}|}{|\mathbf{q} - \mathbf{k}|} \right) + O(\gamma_{d}) 
\sim \frac{1}{\Theta |\mathbf{k}|^{2 - \eta}} + O(\gamma_{d}). \tag{31}$$

Note that at long wave-length fluctuations ( $|\mathbf{k}| \to 0$ ), the summation in (31) will be the dominant factor in the effective bending stiffness (30), compared to the constant  $\kappa_b$ . Thus, at long wave-length fluctuations,  $\kappa_{\rm eff}(\mathbf{k})$  scales as:

$$\kappa^{\text{eff}}(\mathbf{k}) := \Theta |\mathbf{k}|^{-\zeta} \sim \frac{k_B T E}{\Theta |\mathbf{k}|^{2-\zeta}},\tag{32}$$

from which we obtain the effective bending stiffness as:

$$\kappa^{\text{eff}}(\mathbf{k}) \sim \sqrt{Ek_B T} |\mathbf{k}|^{-1}. \tag{33}$$

$${\langle|\overline{h}(\mathbf{k})|^2\rangle} \sim (\sum_i \alpha_i |\mathbf{k}|^{\xi_i})^{-1} = \frac{1}{\alpha_1 |\mathbf{k}|^{\xi_1} + \alpha_2 |\mathbf{k}|^{\xi_2} + \alpha_3 |\mathbf{k}|^{\xi_3} + \alpha_4 |\mathbf{k}|^{\xi_4} + \cdots}$$

where  $\xi_i$  are not necessarily integers. In this case, the dominant modes of the fluctuations are the long wave-length modes, where  $\mathbf{k} \to 0$ . Therefore, the term with smaller exponents  $\xi_i$  in the denominator of the above equation will be the leading term in the summation. Accordingly, we can *approximately* describe the fluctuations in terms of the leading term as:  $\langle \bar{h}(\mathbf{k})^2 \rangle \sim 1/\mathbf{k}^{\xi}$ , with  $\xi$  being the smallest exponent in the denominator of the above equation. In this manner, the effective bending stiffness varies with the fluctuation mode as:  $\mathbf{k}^{\text{eff}}(\mathbf{k}) \sim \mathbf{k}^{\xi-4}$ . We set  $\zeta = 4 - \xi \geqslant 0$  and our goal is to obtain an estimate of  $\zeta$ .

<sup>&</sup>lt;sup>4</sup> In the presence of the nonlinear in-plane strain, the fluctuations can be described more generally as:

The expression for the effective bending stiffness in (33) has been previously derived by Ahmadpoor et al. (2017) for a free fluctuating solid membrane. Using this effective bending stiffness, the fluctuations spectra are given as:

$$\langle |h(\mathbf{k})|^2 \rangle = \frac{k_B T}{L^2(\kappa^{\text{eff}}(\mathbf{k}))|\mathbf{k}|^4 + \gamma_d} \sim \frac{k_B T}{L^2(\sqrt{Ek_B T}|\mathbf{k}|^3 + \gamma_d)},\tag{34}$$

from which the fluctuations formula in real space is obtained as:

$$\langle h^2 \rangle = \sum_{\mathbf{k} \in \mathcal{K}} \langle |h(\mathbf{k})|^2 \rangle \sim \sum_{\mathbf{k} \in \mathcal{K}} \frac{k_B T}{L^2 (\sqrt{E k_B T} |\mathbf{k}|^3 + \gamma_d)}$$

$$\sim \left(\frac{L}{2\pi}\right)^2 \int_0^\infty \frac{k_B T}{L^2 (\sqrt{E k_B T} |\mathbf{k}|^3 + \gamma_d)} 2\pi |\mathbf{k}| d|\mathbf{k}|$$

$$\sim \frac{1}{3\sqrt{3}} \sqrt[3]{\frac{(k_B T)^2}{E \gamma_d}}.$$
(35)

The fluctuations in (35) should be confined within the two hard walls in distance 2d from one another;  $\langle h^2 \rangle < d^2$ . To ensure this inequality, we set  $\langle h^2 \rangle = \xi d^2$ , where  $0 < \xi < 1$ . Solving for  $\gamma_d$ , we have:

$$\langle h^2 \rangle \sim \frac{1}{3\sqrt{3}} \sqrt[3]{\frac{(k_B T)^2}{E \gamma_d}} := \xi d^2, \to \gamma_d \sim \frac{(k_B T)^2}{81\sqrt{3} E d^6 \xi^3}.$$
 (36)

Substituting Eq. (36) for  $\gamma_d$  into the free energy (24), and taking its derivative with respect to the volume of the system to obtain the entropic pressure, we have:

$$p = -\frac{\partial F_0}{\partial V} = -\frac{1}{2L^2} \frac{\partial F_0}{\partial d} = -\frac{1}{2L^2} \frac{\partial F_0}{\partial \gamma_d} \frac{\partial \gamma_d}{\partial d}$$

$$\sim -\frac{1}{2L^2} \left( \sum_{\mathbf{k} \in \mathcal{K}} \frac{k_B T}{(\kappa^{\text{eff}}(\mathbf{k}))|\mathbf{k}|^4 + \gamma_d} \right) \left( -\frac{2(k_B T)^2}{27\sqrt{3}Ed^7 \xi^3} \right)$$

$$\sim \frac{1}{L^2} \left( L^2 \langle h^2 \rangle \right) \left( \frac{(k_B T)^2}{27\sqrt{3}Ed^7 \xi^3} \right) \sim \xi d^2 \left( \frac{(k_B T)^2}{27\sqrt{3}Ed^7 \xi^3} \right)$$

$$\sim \frac{(k_B T)^2}{27\sqrt{3}E\xi^2} \left( \frac{1}{d^5} \right). \tag{37}$$

The entropic force on a confined fluctuating solid membrane scales as  $p \propto 1/d^5$  for large values of d. We now return our attention to the second case; small intermembrane distances, where entropic force is indeed large enough to suppress the nonlinearities. To start, let us calculate the summation in (30), assuming that  $\gamma_d$  is not small and cannot be neglected.

$$\frac{1}{L^{2}} \sum_{\mathbf{q} \in \mathcal{K}} \left( \frac{\kappa^{\text{eff}}(\mathbf{q} - \mathbf{k}) \left( \kappa^{\text{eff}}(\mathbf{k}) |\mathbf{k}|^{4} + \gamma_{d} \right) \left( \sin \theta_{\mathbf{q}, \mathbf{k}} \right)^{4}}{\kappa^{\text{eff}}(\mathbf{k}) \left( \kappa^{\text{eff}}(\mathbf{q} - \mathbf{k}) |\mathbf{q} - \mathbf{k}|^{4} + \gamma_{d} \right)^{2}} \left| \frac{\mathbf{q} - \mathbf{k}}{\mathbf{k}} \right|^{3} + \frac{\left( \sin \theta_{\mathbf{q}, \mathbf{k}} \right)^{4}}{\kappa^{\text{eff}}(\mathbf{q} - \mathbf{k}) |\mathbf{q} - \mathbf{k}|^{4} + \gamma_{d}} \right) \\
\sim \frac{1}{L^{2}} \sum_{\mathbf{q} \in \mathcal{K}} \left( \frac{|\mathbf{q} - \mathbf{k}|^{3-\eta} \left( \Theta |\mathbf{k}|^{4-\eta} + \gamma_{d} \right) \left( \sin \theta_{\mathbf{q}, \mathbf{k}} \right)^{4}}{|\mathbf{k}|^{3-\eta} \left( \Theta |\mathbf{q} - \mathbf{k}|^{4-\eta} + \gamma_{d} \right)^{2}} + \frac{\left( \sin \theta_{\mathbf{q}, \mathbf{k}} \right)^{4}}{\Theta |\mathbf{q} - \mathbf{k}|^{4-\eta} + \gamma_{d}} \right) \\
\sim \frac{c_{1} \theta |\mathbf{k}|^{6-\eta}}{\gamma_{d}^{2} (5 - \eta)} + \frac{c_{2} |\mathbf{k}|^{2}}{\gamma_{d}} \tag{38}$$

which clearly vanishes at long wave-length fluctuations, i.e.  $|\mathbf{k}| \to 0$ . Thus, the effective bending stiffness  $\kappa^{\rm eff}(\mathbf{k})$  for this case is independent of mode  $\mathbf{k}$  and converges to a constant:  $\kappa^{\rm eff}(\mathbf{k}) \sim \mathcal{C}$ . The fluctuations in each mode are then given by:

$$\langle |h(\mathbf{k})|^2 \rangle = \frac{k_B T}{L^2 (C|\mathbf{k}|^4 + \gamma_d)},\tag{39}$$

from which the fluctuations in real space are obtained as:

$$\langle h^2 \rangle = \sum_{\mathbf{k} \in \mathcal{K}} \langle |h(\mathbf{k})|^2 \rangle \sim \sum_{\mathbf{k} \in \mathcal{K}} \frac{k_B T}{L^2 (C |\mathbf{k}|^4 + \gamma_d)}$$

$$\sim \left(\frac{L}{2\pi}\right)^2 \int_0^\infty \frac{k_B T}{L^2 (C |\mathbf{k}|^4 + \gamma_d)} 2\pi |\mathbf{k}| d|\mathbf{k}|$$

$$= \frac{k_B T}{8\sqrt{C\gamma_d}}.$$
(40)

Solving  $\langle h^2 \rangle = \xi d^2$  for  $\gamma_d$ , we obtain:

$$\langle h^2 \rangle = \frac{k_B T}{8\sqrt{C\gamma_d}} := \xi d^2, \quad \rightarrow \quad \gamma_d = \frac{(k_B T)^2}{64C\xi^2 d^4}. \tag{41}$$

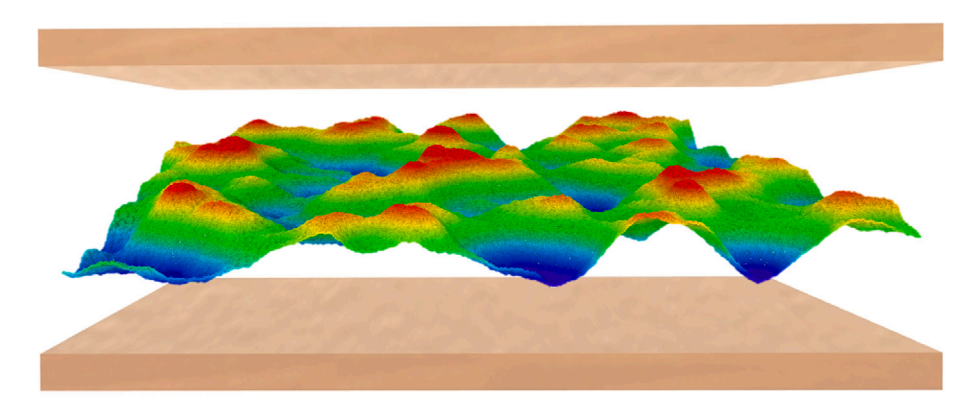


Fig. 3. Molecular dynamics simulation of a fluctuating graphene sheet confined between two hard walls.

Substituting Eq. (41) for  $\gamma_d$  into the free energy (24), and taking its derivative with respect to the volume of the system to obtain the entropic pressure, we have:

$$p = -\frac{\partial F_0}{\partial V} = -\frac{1}{2L^2} \frac{\partial F_0}{\partial d} = -\frac{1}{2L^2} \frac{\partial F_0}{\partial \gamma_d} \frac{\partial \gamma_d}{\partial d}$$

$$\sim -\frac{1}{2L^2} \left( \sum_{\mathbf{k} \in \mathcal{K}} \frac{k_B T}{C|\mathbf{k}|^4 + \gamma_d} \right) \left( -\frac{(k_B T)^2}{16Cd^5 \xi^2} \right) \sim \frac{1}{L^2} \left( L^2 \langle h^2 \rangle \right) \left( \frac{(k_B T)^2}{16Cd^5 \xi^2} \right)$$

$$\sim \xi d^2 \left( \frac{(k_B T)^2}{16Cd^5 \xi^2} \right) \sim \frac{(k_B T)^2}{16\xi C} \left( \frac{1}{d^3} \right). \tag{42}$$

The entropic pressure for this case scales as  $p \sim 1/d^3$ . This power law has been previously derived for fluid membranes within linear elasticity. In the following section, we perform molecular dynamics simulations to verify our theoretical findings.

### 5. Molecular dynamics simulation

The MD simulation model is schematically shown in Fig. 3, where a graphene membrane is sandwiched between two rigid walls. The steric pressure acting on the graphene due to geometric confinement is modeled by a repulsive wall potential:

$$E(\delta) = \frac{2\epsilon}{15} \left(\frac{\sigma}{\delta}\right)^9,\tag{43}$$

where  $\delta$  is the distance between atoms and wall and  $\epsilon$  and  $\sigma$  are constants that control the repulsion magnitude. This potential is adopted from the repulsive component of the Lennard Jones potential implemented in LAMMPS, however, it does not characterize the Van der Waals forces acting between the graphene and the wall. To isolate the effects of steric pressure, the model intentionally disregards the attractive part of the Van der Waals force. The simulation box is periodic in the lateral directions, and its dimension is determined by the size of the graphene sheet. At finite temperatures, ripples are formed in graphene due to thermal fluctuations. To restrain free thermal fluctuations within a domain with height d between two walls, a "repulsion zone", with a height of 0.3 nm, is positioned adjacent to the top and bottom walls. Inside the zone, the graphene experiences the repulsive potential. Outside the zone, the graphene is allowed to fluctuate freely.

The parameters in the repulsive potential are chosen to simulate the repulsive forces akin to the elastic collision experienced when atoms interact with the walls. This is analogous to the elastic collision that occurs when ideal gas atoms interact with the walls of a container, resulting in a pressure that adheres to the ideal gas law, which can be used to calibrate the repulsive parameters. The calibration of parameters is performed in a similar simulation model where ideal gas atoms (replacing the graphene) are inserted between the walls, as shown in Fig. D.6. The gas pressure exerted by the walls is computed by varying the value of  $\sigma$  while keeping  $\epsilon$  constant at 1 eV. As shown in Fig. D.7, it is found that  $\sigma = 2.5$  Å results in pressures that align with the ideal gas law. Therefore,  $\sigma = 2.5$  Å and  $\epsilon = 1$  eV are chosen to mimic the elastic collision between the wall and confining atoms in the calculation of the steric pressure of graphene.

The MD simulations in this study are conducted within the NVT ensemble, employing a Nose–Hoover thermostat for temperature control with a time step of 0.1 fs. The size of the graphene sheet is chosen to be 40 by 40 nm, and the temperature for the MD simulation is set at 1000 K. These parameters are selected to intensify the thermal rippling of graphene, which in turn facilitates a reduction in sampling time during the MD simulation. The steric pressure exerted by the wall is calculated by  $p = \langle f \rangle / A$ , where  $\langle f \rangle$  is the time-averaged reaction force from the wall and A is the cross-section area.

Fig. 4(a) and (c) displays the pressure obtained from MD simulations for two extreme separations considered in this study. It is noted that larger separations exhibit increased fluctuations, suggesting the need for extended sampling time to attain a more accurate ensemble average. The averaged steric pressure values for the top and bottom walls are found to be almost identical. Fig. 4(b) and

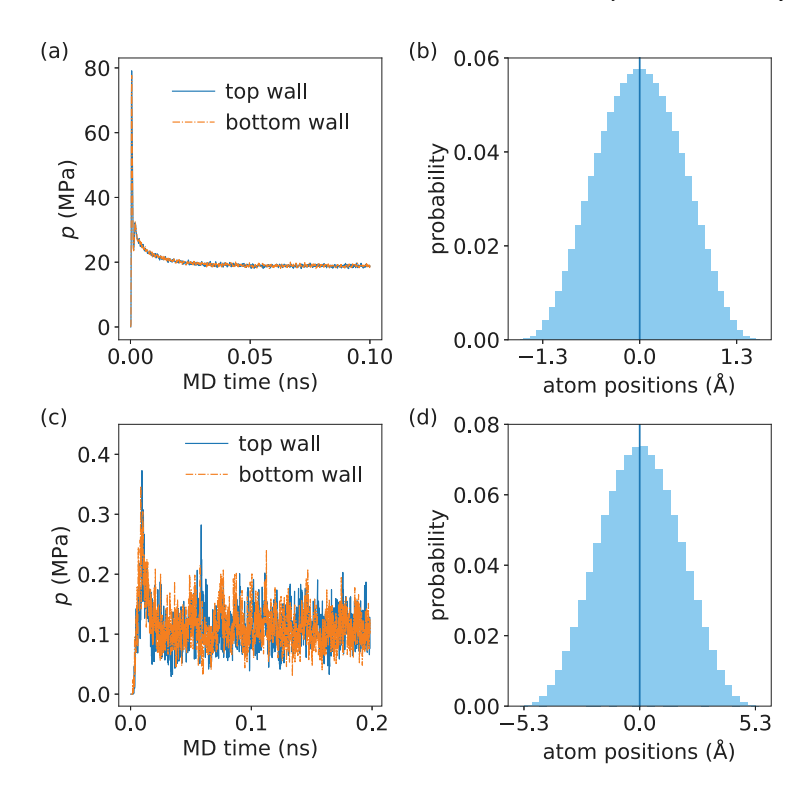


Fig. 4. Steric pressure and probability density of vertical positions of graphene atoms for separation distance 1.3 Å (a, b) and 5.3 Å (c, d).

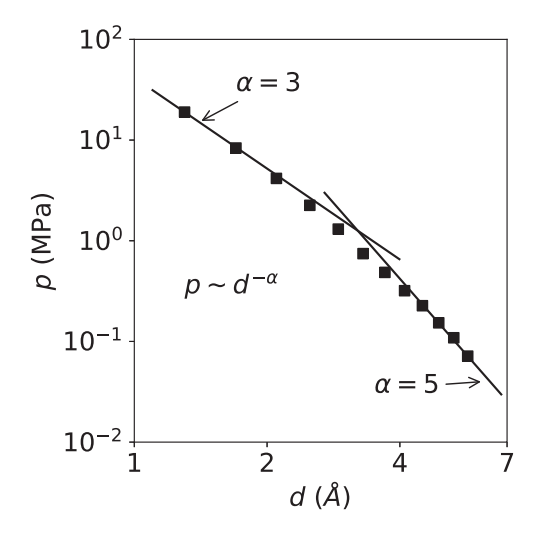


Fig. 5. Steric pressure p, as a function of the distance d between two hard walls.

(d) show the histograms representing the positions of graphene atoms during the MD simulations. The histograms confirm that all the atoms are effectively confined by the walls within the free fluctuation zone. In the case of the smallest separation 1.3 Å, there is a minimal probability of atoms moving beyond the bounding walls.

The steric pressure is plotted as a function of the separation distance in Fig. 5. At short separation distances, only small out-of-plane fluctuations are allowed in the graphene. In this case, the in-plane and out-of-plane modes can be decoupled under a harmonic approximation (Gao and Huang, 2014). Consequently, the pressure follows the scaling law proposed by Helfrich (1978), where  $p \sim d^{-3}$ . At a large separation, the strong anharmonic effect of graphene dominates the thermal fluctuations, resulting in a different scaling law, that is,  $p \sim d^{-5}$ . A transition from harmonic to anharmonic behavior is observed between these two extremities.

#### 6. Summary and conclusion

In this paper, we have presented a statistical mechanics model within a fully nonlinear elasticity framework to study the entropic force on confined fluctuating solid membranes. To deal with nonlinearity, we used a variational perturbation method to derive closed-form approximate expressions for the entropic force. Our results indicate a different power law for the entropic pressure, compared to that of fluid membranes. Specific outcomes of the work are as follows:

- For small values of confining distance d, the entropic pressure is expected to be large enough to suppress the effects of nonlinearities. In this case, the solid membranes essentially behave as linear elastic sheets. Thus, the resulting power law for the entropic force is the same as that of a fluid membrane, i.e.,  $p \propto 1/d^3$ .
- For large values of d, the entropic force will be smaller to a degree that cannot suppress the nonlinearities. In this case, the power law for the entropic force is derived as  $p \propto 1/d^5$  and decays faster, compared to small values of d.
- The entropic force has been studied for fluid membranes in computational models in the past. In this work, we revisited this problem for solid membranes using molecular dynamics simulations. We have used graphene as a representative of solid membranes. Our results from simulations are in agreement with the theoretical predictions and show two different regions for the variations of the scaling laws for the entropic force with a crossover distance of about 3.5Å.

Finally, we note that, while we used graphene as a *proof of concept*, the results are applicable to any other solid membranes in biology or among crystalline membranes. A detailed physical consequence of our study is beyond the scope of this work, but we anticipate its implication in numerous biological phenomena as well as applications of crystalline membranes in the design of novel flexible nanostructures.

#### CRediT authorship contribution statement

**Rubayet Hassan:** Formal analysis, Methodology, Validation, Investigation, Writing – original draft. **Maria Alejandra Garzon:** Formal analysis, Investigation, Methodology, Validation, Writing – original draft. **Wei Gao:** Conceptualization, Funding acquisition, Supervision, Writing – review & editing. **Fatemeh Ahmadpoor:** Conceptualization, Funding acquisition, Supervision, Writing – review & editing.

#### **Declaration of competing interest**

The authors declare the following financial interests/personal relationships which may be considered as potential competing interests: Fatemeh Ahmadpoor reports financial support was provided by National science Foundation (US). Wei Gao reports financial support was provided by National science Foundation (US). Rubayet Hassan reports financial support was provided by National science Foundation (US). Maria Alejandra Garzon reports financial support was provided by National science Foundation (US). If there are other authors, they declare that they have no known competing financial interests or personal relationships that could have appeared to influence the work reported in this paper.

#### Data availability

Data will be made available on request.

#### Acknowledgments

F.A. and R.H. gratefully acknowledge financial support from New Jersey Institute of Technology and the National Science Foundation, United States through Grant No. CMMI-2237530. W.G. and M.G. gratefully acknowledge the financial support of this work by the National Science Foundation, United States through Grant No. CMMI-2308163 and CMMI-2305529. The authors acknowledge the Texas Advanced Computing Center (TACC) at the University of Texas at Austin for providing HPC resources that have contributed to the research results reported within this paper. All authors approved the version of the manuscript to be published.

# Appendix A. Fourier transformation

Fourier transformation can be expressed in terms of sinusoidal functions as:

$$u_{\scriptscriptstyle X}(x) = \sum_{q \in \mathcal{K}_1} a_q \cos(qx) + b_q \sin(qx) \tag{A.1}$$

On the other hand, given that  $\overline{u}^{Re}(q)$  and  $\overline{u}^{Im}(q)$  are the real and imaginary parts of the  $\overline{u}(q)$  we can expand the complex Fourier transform as:

$$u_{\scriptscriptstyle X}(x) = \sum_{q \in \mathcal{K}_1} \overline{u}(q) \mathbf{e}^{\iota q \cdot x}$$

$$\begin{split} &= \sum_{q \in \mathcal{K}_1} (\overline{u}^{\text{Re}}(q) + \mathrm{i}\overline{u}^{\text{Im}}(q))(\cos(qx) + \mathrm{i}\sin(qx)) \\ &= \sum_{q \in \mathcal{K}_1} \overline{u}^{\text{Re}}(q)\cos(qx) - \overline{u}^{\text{Im}}(q)\sin(qx) + \mathrm{i}\sum_{q \in \mathcal{K}_1} (\overline{u}^{\text{Im}}(q)\cos(qx) + \overline{u}^{\text{Re}}(q)\sin(qx)) \end{split} \tag{A.2}$$

We note that for each mode q, there is a conjugate mode -q, for which we have:  $\overline{u}^{\mathrm{Im}}(-q) = -\overline{u}^{\mathrm{Im}}(q)$ ,  $\overline{u}^{\mathrm{Re}}(-q) = \overline{u}^{\mathrm{Re}}(q)$ ,  $\cos(-qx) = \cos(qx)$ , and  $\sin(-qx) = -\sin(qx)$  which causes the imaginary part of the above summation to vanish. Comparing this summation with the expansion in (A.1), we can readily relate the coefficients as:  $a_q = \overline{u}^{\mathrm{Re}}(q)$  and  $b_q = -\overline{u}^{\mathrm{Im}}(q)$ .

The derivatives and their corresponding integrations in one-dimensional problem can be expressed in Fourier expansion as below:

$$\frac{\partial u_x}{\partial x} = \sum_{q \in \mathcal{K}_1} i \, q \overline{u}(q) \mathbf{e}^{iq \cdot x}, \qquad \int \left(\frac{\partial u_x}{\partial x}\right) = 0, \qquad \int \left(\frac{\partial u_x}{\partial x}\right)^2 = L^2 \sum_{q \in \mathcal{K}_1} q^2 |\overline{u}(q)|^2, \qquad (A.3a)$$

$$\int \left(\frac{\partial^2 h}{\partial x^2}\right)^2 = L^2 \sum_{q \in \mathcal{K}_1} q^4 |\overline{h}(q)|^2, \qquad \int \left(\frac{\partial h}{\partial x}\right)^4 = L^2 \sum_{q \in \mathcal{K}_1} |\overline{A}(q)|^2$$
(A.3b)

$$\int \frac{\partial u_x}{\partial x} \left(\frac{\partial h}{\partial x}\right)^2 = L^2 \sum_{q \in \mathcal{K}_1} i \, q \overline{u}(q) \overline{A}(-q) = L^2 \sum_{q \in \mathcal{K}_1} i \, q (\overline{u}^{Re}(q) + i \, \overline{u}^{Im}(q)) (\overline{A}^{Re}(-q) + i \, \overline{A}^{Im}(-q))$$

$$= L^2 \sum_{q \in \mathcal{K}_1} i \, q (\overline{u}^{Re}(q) + i \, \overline{u}^{Im}(q)) (\overline{A}^{Re}(q) - i \, \overline{A}^{Im}(q))$$

$$= L^2 \sum_{q \in \mathcal{K}_1} q \left(\overline{u}^{Re}(q) \overline{A}^{Im}(q) - \overline{u}^{Im}(q) \overline{A}^{Re}(q)\right)$$
(A.3c)

The superscripts "Re" and "Im" denote the decomposition into real and imaginary parts. Also, note that we have dropped the imaginary part of the above summation since it vanishes by summing over the conjugate modes.

For the 2D case, the corresponding Fourier transformation has real and imaginary parts; i.e.  $\overline{u}(q) = \overline{u}^{Re}(q) + i \overline{u}^{Im}(q)$ , in which the superscripts denote the real and imaginary parts. The corresponding conjugate of each mode is also derived as:  $\overline{u}^*(q) = \overline{u}(-q) = \overline{u}^{Re}(q) - i \overline{u}^{Im}(q)$ , where  $\overline{u}(q)\overline{u}^*(q) = |\overline{u}(q)|^2$ . Further, we remark on the orthogonality property of the Fourier modes:

$$\int \overline{u}_{\gamma}(\mathbf{q})\overline{u}_{\delta}(\mathbf{q}')e^{i(\mathbf{q}+\mathbf{q}')\cdot\mathbf{x}}d\mathbf{x} = \delta_{\mathbf{q},-\mathbf{q}'}\overline{u}_{\gamma}(\mathbf{q})\overline{u}_{\delta}(\mathbf{q}')L^{2}$$

$$= \overline{u}_{\gamma}(\mathbf{q})\overline{u}_{\delta}(-\mathbf{q})L^{2}$$
(A.4)

Similar arguments can be made for  $\overline{A}_{\gamma\delta}(\mathbf{q})$  and  $\overline{w}(\mathbf{q})$ . Now we can calculate the integration of each term in  $U_{\rm h}$ ,  $U_{\rm ac}$  and  $U_{\rm anh}$  in Fourier space. In the following equations, we demonstrate the details of the Fourier transformation of these terms that were not shown in the main text of the paper:

$$\int_{\mathbb{S}} \left( \frac{\partial u_{\gamma}}{\partial x_{\delta}} \right)^{2} d\mathbf{x} = L^{2} \sum_{\mathbf{q} \in \mathcal{K}} q_{\delta}^{2} |\overline{u}_{\gamma}(\mathbf{q})|^{2}$$
(A.5a)

$$\int_{\mathbb{S}} \left( \frac{\partial h}{\partial x_{\gamma}} \frac{\partial h}{\partial x_{\delta}} \right)^{2} d\mathbf{x} = L^{2} \sum_{\mathbf{q} \in \mathcal{K}} \left| \overline{A}_{\gamma \delta}(\mathbf{q}) \right|^{2}$$

$$\int_{\mathbb{S}} \left( \frac{\partial u_{\gamma}}{\partial x_{\delta}} \frac{\partial h}{\partial x_{k}} \frac{\partial h}{\partial x_{l}} \right) d\mathbf{x} = L^{2} \sum_{\mathbf{q} \in \mathcal{K}} \mathbf{i} \ q_{\delta} \overline{u}_{\gamma}(\mathbf{q}) \overline{A}_{kl}(-\mathbf{q})$$
(A.5b)

$$+\mathbf{i} \left( \overline{A}_{kl}^{\text{Re}}(\mathbf{q}) \overline{u}_{\gamma}^{\text{Re}}(\mathbf{q}) + \overline{u}_{\gamma}^{\text{Im}}(\mathbf{q}) \overline{A}_{kl}^{\text{Im}}(\mathbf{q}) \right)$$

$$= L^{2} \sum_{r \in \Gamma} q_{\delta} \left\{ \overline{A}_{kl}^{\text{Im}}(\mathbf{q}) \overline{u}_{\gamma}^{\text{Re}}(\mathbf{q}) - \overline{u}_{\gamma}^{\text{Im}}(\mathbf{q}) \overline{A}_{kl}^{\text{Re}}(\mathbf{q}) \right\}$$
(A.5c)

Note that for each  $\mathbf{q}$  mode in the summation, there is a conjugate of  $-\mathbf{q}$ , that makes the imaginary part of the summation in (A.5c) vanish:

 $=L^2\sum_{\mathbf{q},\delta}q_{\delta}\left\{\overline{A}_{kl}^{\mathrm{Im}}(\mathbf{q})\overline{u}_{\gamma}^{\mathrm{Re}}(\mathbf{q})-\overline{u}_{\gamma}^{\mathrm{Im}}(\mathbf{q})\overline{A}_{kl}^{\mathrm{Re}}(\mathbf{q})\right.$ 

$$\begin{split} q_{\delta}\left(\overline{A}_{kl}^{\text{Re}}(\mathbf{q})\overline{u}_{\gamma}^{\text{Re}}(\mathbf{q}) + \overline{u}_{\gamma}^{\text{Im}}(\mathbf{q})\overline{A}_{kl}^{\text{Im}}(\mathbf{q})\right) + (-q_{\delta})\left(\overline{A}_{kl}^{\text{Re}}(-\mathbf{q})\overline{u}_{\gamma}^{\text{Re}}(-\mathbf{q}) + \overline{u}_{\gamma}^{\text{Im}}(-\mathbf{q})\overline{A}_{kl}^{\text{Im}}(-\mathbf{q})\right) \\ &= q_{\delta}\left(\overline{A}_{kl}^{\text{Re}}(\mathbf{q})\overline{u}_{\gamma}^{\text{Re}}(\mathbf{q}) + \overline{u}_{\gamma}^{\text{Im}}(\mathbf{q})\overline{A}_{kl}^{\text{Im}}(\mathbf{q})\right) - q_{\delta}\left(\overline{A}_{kl}^{\text{Re}}(\mathbf{q})\overline{u}_{\gamma}^{\text{Re}}(\mathbf{q}) + (-\overline{u}_{\gamma}^{\text{Im}}(\mathbf{q}))(-\overline{A}_{kl}^{\text{Im}}(\mathbf{q}))\right) \\ &= 0 \end{split} \tag{A.6}$$

Since there will not be any contribution from the imaginary parts of the summations to the free energy, we have taken them out from our calculations.

#### Appendix B. Effective strain energy

The effective strain energy, which consists of the remainder terms in the exponent of the partition function integral once the in-plane terms have been integrated out, can be expressed as:

$$U_s^{\text{eff}} = \frac{1}{4} E \sum_{\mathbf{q} \in \mathcal{K}} \Psi(\mathbf{q}) \Psi^*(\mathbf{q})$$
(B.1)

in which, for ease of notation, we have defined  $\Psi(\mathbf{q})$  as:

$$\Psi(\mathbf{q}) = \frac{1}{\mathbf{q}^2} \left\{ q_y^2 \overline{A}_{xx}(\mathbf{q}) + q_x^2 \overline{A}_{yy}(\mathbf{q}) - 2q_x q_y \overline{A}_{xy}(\mathbf{q}) \right\}$$
(B.2)

Furthermore, we can more compactly express the strain energy using the so-called transverse projector operator (Nelson et al., 2004) as below:

$$\Psi(\mathbf{q}) = P_{ii}^{T}(\mathbf{q}) \overline{A}_{ii}(\mathbf{q}) \tag{B.3}$$

in which

$$P_{ij}^{T}(\mathbf{q}) = \delta_{ij} - \frac{q_i q_j}{\mathbf{q}^2} \tag{B.4}$$

Note that  $\Psi(\mathbf{q})\Psi^*(\mathbf{q}) = \Psi(\mathbf{q})\Psi(-\mathbf{q}) = |\Psi(\mathbf{q})|^2$  and is expanded as follows:

$$\begin{split} \Psi(\mathbf{q})\Psi(-\mathbf{q}) &= |\Psi(\mathbf{q})|^2 \\ &= \frac{1}{(q_x^2 + q_y^2)^2} \left\{ q_x^4 \overline{A}_{yy}^{\text{Re}}(\mathbf{q})^2 + q_x^4 \overline{A}_{yy}^{\text{Im}}(\mathbf{q})^2 + q_y^4 \overline{A}_{xx}^{\text{Re}}(\mathbf{q})^2 + q_y^4 \overline{A}_{xx}^{\text{Im}}(\mathbf{q})^2 \\ &- 4q_x q_y^3 \overline{A}_{xx}^{\text{Im}}(\mathbf{q}) \overline{A}_{xy}^{\text{Im}}(\mathbf{q}) + 2q_x^2 q_y^2 \overline{A}_{xx}^{\text{Im}}(\mathbf{q}) \overline{A}_{yy}^{\text{Im}}(\mathbf{q}) - 4q_x^3 q_y \overline{A}_{xy}^{\text{Im}}(\mathbf{q}) \overline{A}_{yy}^{\text{Im}}(\mathbf{q}) \\ &+ 4q_x^2 q_y^2 \overline{A}_{xy}^{\text{Im}}(\mathbf{q})^2 + q_x^4 \overline{A}_{yy}^{\text{Im}}(\mathbf{q})^2 + q_y^4 \overline{A}_{xx}^{\text{Im}}(\mathbf{q})^2 - 4q_x q_y^3 \overline{A}_{xx}^{\text{Re}}(\mathbf{q}) \overline{A}_{xy}^{\text{Re}}(\mathbf{q}) \\ &+ 2q_x^2 q_y^2 \overline{A}_{xx}^{\text{Re}}(\mathbf{q}) \overline{A}_{yy}^{\text{Re}}(\mathbf{q}) - 4q_x^3 q_y \overline{A}_{xy}^{\text{Re}}(\mathbf{q}) \overline{A}_{yy}^{\text{Re}}(\mathbf{q}) + 4q_x^2 q_y^2 \overline{A}_{xy}^{\text{Re}}(\mathbf{q})^2 \right\} \end{split}$$

# Appendix C. The variational perturbation theory and the ensemble averages

Consider the nonlinear energy in (20). The idea is that the nonlinear part is a small perturbation compared to the quadratic functional  $\mathcal{H}_0$ . Let F, be the free energy of the system. In the absence of the nonlinear perturbation term  $\mathcal{H}_p$ , the partition function  $Z_0$  and free energy  $F_0$  can be easily obtained using standard Gaussian integrations. The effect of the nonlinear term on the total free energy of the system can be then estimated by a perturbation expansion around  $F_0$ . We start with expanding the partition function of the system Z:

$$Z = \int \exp(-\beta(\mathcal{H}_0 + \mathcal{H}_p))D[w] = Z_0 \langle \exp(-\beta\mathcal{H}_p) \rangle_{\mathcal{H}_0}$$
 (C.1)

wherein  $\beta = \frac{1}{k_B T}$  and the subscript  $\langle \cdot \rangle_{\mathcal{H}_0}$  denotes ensemble average, with respect to  $\mathcal{H}_0$ . The exponential term in the above equation can be expanded in a Taylor series as:

$$\exp(-\beta \mathcal{H}_p) = 1 - \beta \mathcal{H}_p + \frac{1}{2}(\beta \mathcal{H}_p)^2 + \dots = \sum_{n=0}^{\infty} \frac{(-\beta \mathcal{H}_p)^n}{n!}$$
(C.2)

Then the free energy of the system is obtained as:

$$F = -\frac{1}{\beta} \log Z = F_0 - \frac{1}{\beta} \log(1 + \sum_{n=1}^{\infty} \frac{\langle (-\beta \mathcal{H}_p)^n \rangle_{\mathcal{H}_0}}{n!})$$
 (C.3)

Expanding the logarithm term we have:

$$\log\left(\sum_{n=0}^{\infty} \frac{(-\beta)^n \langle \mathcal{H}_p^n \rangle_{\mathcal{H}_0}}{n!}\right) = \left(\sum_{n=1}^{\infty} \frac{(-\beta)^n \langle \mathcal{H}_p^n \rangle_{\mathcal{H}_0}}{n!}\right) - \frac{1}{2} \left(\sum_{n=1}^{\infty} \frac{(-\beta)^n \langle \mathcal{H}_p^n \rangle_{\mathcal{H}_0}}{n!}\right)^2 + \cdots$$
(C.4)

and hence, the free energy expansion can be derived to be:

$$F = F_0 - \frac{1}{\beta} \sum_{n=1}^{\infty} \frac{(-\beta)^n}{n!} \langle \mathcal{H}_p^n \rangle_{\mathcal{H}_0}^c$$
 (C.5)

where the superscript  $\langle \cdot \rangle^c$  denotes the cumulant averages. The cumulant averages, up to fourth order, are:

$$\langle \mathcal{H}_p \rangle_{\mathcal{H}_0}^c = \langle \mathcal{H}_p \rangle_{\mathcal{H}_0}$$

R. Hassan et al.

$$\begin{split} \langle \mathcal{H}_p^2 \rangle_{\mathcal{H}_0}^c &= \langle \mathcal{H}_p^2 \rangle_{\mathcal{H}_0} - \langle \mathcal{H}_p \rangle_{\mathcal{H}_0}^2 \\ \langle \mathcal{H}_p^3 \rangle_{\mathcal{H}_0}^c &= \langle \mathcal{H}_p^3 \rangle_{\mathcal{H}_0} - 3 \langle \mathcal{H}_p^2 \rangle_{\mathcal{H}_0} \langle \mathcal{H}_p \rangle_{\mathcal{H}_0} + 2 \langle \mathcal{H}_p \rangle_{\mathcal{H}_0}^3 \\ \langle \mathcal{H}_p^4 \rangle_{\mathcal{H}_0}^c &= \langle \mathcal{H}_p^4 \rangle_{\mathcal{H}_0} - 3 \langle \mathcal{H}_p^2 \rangle_{\mathcal{H}_0} \langle \mathcal{H}_p \rangle_{\mathcal{H}_0} - 3 \langle \mathcal{H}_p^2 \rangle_{\mathcal{H}_0}^2 + 12 \langle \mathcal{H}_p^2 \rangle_{\mathcal{H}_0} \langle \mathcal{H}_p \rangle_{\mathcal{H}_0}^2 - 6 \langle \mathcal{H}_p \rangle_{\mathcal{H}_0}^4 \end{split}$$

Accordingly, the excess free energy can be related to the total average energy of the system up to nth order as:

$$\langle \mathcal{H} \rangle = \langle \mathcal{H}_0 \rangle_{\mathcal{H}_0} + \frac{1}{\beta} \sum_{n=1}^{\infty} \frac{(-\beta)^n}{n!} \langle \mathcal{H}_p^n \rangle_{\mathcal{H}_0}^c$$

The infinite series in the above equation gives us the exact average amount of energy that the nonlinear term adds to the system. In practice, however, we need to truncate the series to some finite order. If the nonlinear term is small (and the series is well-behaved), we can expect to achieve a reasonable estimate by evaluating the first few terms of perturbation expansion in Eq. (C.5). Yet, it has been shown that the effect of nonlinearities in solid membranes such as graphene is indeed remarkable and the naive perturbation method does not provide a reasonable estimate for the free energy and fluctuations (Ahmadpoor et al., 2017).

To improve the results of what can be obtained from the naive perturbation approach, we adopt an alternative version of it that is rooted in a variational argument. The key idea was first introduced by Kleinert (2009) in the context of anharmonic Hamiltonians arising in quantum mechanics. We briefly elaborate on the details of the procedure here. We start with adding and subtracting a trial Hamiltonian to the nonlinear energy formulation in Eq. (20). In order to describe the out-of-plane fluctuations, consider a trial Hamiltonian as:

$$U_{\text{trial}} = \frac{1}{2} L^2 \sum_{\mathbf{k} \in \mathcal{K}} (\kappa^{\text{eff}}(\mathbf{k}) \mathbf{k}^4 + \gamma_d) |h(\mathbf{k})|^2$$
(C.6)

where  $\kappa^{\rm eff}$  is the unknown effective bending stiffness in general mode-dependent form. Then, the total elastic energy can be written as:

$$U_b + U_s^{\text{eff}} = U_{\text{trial}} + (U_b + U_s^{\text{eff}} - U_{\text{trial}}) \tag{C.7}$$

Then the perturbation expansion of the free energy associated with the Hamiltonian in (C.7) is obtained by the Taylor series in (C.5):

$$F_{\infty} = F_0 - \frac{1}{\beta} \sum_{N=1}^{\infty} \frac{(-\beta)^N}{N!} \langle \left[ U_b + U_s^{\text{eff}} - U_{\text{trial}} \right]^N \rangle_{U_{\text{trial}}}^c$$
(C.8)

where  $F_0$  is the free energy corresponding to the trial Hamiltonian  $U_{\mathrm{trial}}$ :

$$F_{0} = \sum_{\mathbf{k} \in \mathcal{K}} \frac{1}{2\beta} \left( \log(\frac{L^{2}}{2\pi}) + \log(\beta(\kappa^{\text{eff}}(\mathbf{k})|\mathbf{k}|^{4} + \gamma_{d})) \right)$$

$$= C_{F} + \sum_{\mathbf{k} \in \mathcal{K}} \frac{k_{B}T}{2} \log(\kappa^{\text{eff}}(\mathbf{k})|\mathbf{k}|^{4} + \gamma_{d})$$
(C.9)

where we called the first term  $C_F$ , a coefficient that is independent of the effective stiffness  $\kappa^{\rm eff}({\bf k})$ . Needless to say the full expansion in (C.8) as  $N\to\infty$  should be independent of the choice of the trial Hamiltonian. In practice, however, the series is truncated up to a finite order M to obtain an estimate of the free energy. Unlike the infinite series expansion in Eq. (C.8), the truncated series  $F_M$  does depend on the choice of the trial Hamiltonian  $\mathcal{H}_{\rm trial}$ . Accordingly, in order to obtain an optimized estimate, we need to minimize the *sensitivity* of the truncated series to the trial Hamiltonian. To this end, we set (Kleinert, 2009):

$$\frac{\partial F_M}{\partial \kappa^{\text{eff}}(\mathbf{k})} := 0. \tag{C.10}$$

In a rather good approximation, the result for the truncated series of the variational free energy from this method will converge i.e.  $F_M \approx F_{M+1}$  and achieves its minimal sensitivity to the trial function. Up to the first order, the ensemble averages are calculated as:

$$\langle U \rangle = \left\langle \frac{1}{2} \kappa_b L^2 \sum_{\mathbf{k} \in \mathcal{K}} \mathbf{k}^4 |\overline{h}(\mathbf{k})|^2 + \frac{1}{2} L^2 \sum_{\mathbf{k} \in \mathcal{K}} \gamma_d |\overline{h}(\mathbf{k})|^2 \right\rangle_{U_{\text{trial}}} + \left\langle \frac{1}{2} E L^2 \sum_{\mathbf{q} \in \mathcal{K}} |\frac{1}{2} P_{ij}^T(\mathbf{q}) \overline{A}_{ij}(\mathbf{q})|^2 \right\rangle_{U_{\text{trial}}}$$

$$:= \frac{L^2}{2} \sum_{\mathbf{k} \in \mathcal{K}} (\kappa_{\text{eff}}(\mathbf{k}) |\mathbf{k}|^4 + \gamma_d) \langle |\overline{h}(\mathbf{k})|^2 \rangle_{U_{\text{trial}}}$$
(C.11)

To calculate the averages in Eq. (C.11), we start by expanding the out-of-plane displacement field in Fourier space:

$$\frac{\partial h}{\partial x_i} \frac{\partial h}{\partial x_j} = \sum_{\mathbf{k}, \mathbf{k}' \in \mathcal{K}} -k_i k'_j \overline{h}(\mathbf{k}) \overline{h}(\mathbf{k}') e^{i(\mathbf{k} + \mathbf{k}') \cdot \mathbf{x}}$$

$$= \sum_{\mathbf{k}, \mathbf{q} \in \mathcal{K}} -k_i (q_j - k_j) \overline{h}(\mathbf{k}) \overline{h}(\mathbf{q} - \mathbf{k}) e^{i\mathbf{q} \cdot \mathbf{x}} = \sum_{\mathbf{q} \in \mathcal{K}} \overline{A}_{ij}(\mathbf{q}) e^{i\mathbf{q} \cdot \mathbf{x}} \tag{C.12a}$$

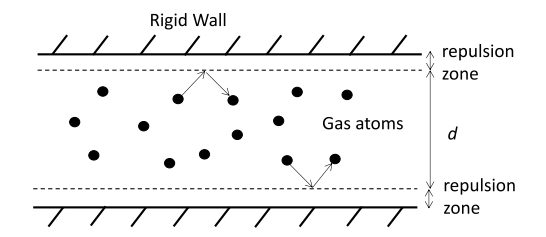


Fig. D.6. Computation model of molecular dynamics simulation.

in which:

$$\overline{A}_{ij}(\mathbf{q}) = \sum_{\mathbf{k} \in \mathcal{K}} -k_i (q_j - k_j) \overline{h}(\mathbf{k}) \overline{h}(\mathbf{q} - \mathbf{k})$$
(C.13)

After substituting the operator  $P_{i:}^{T}(\mathbf{q})$ , we obtain:

$$P_{ij}^{T}(\mathbf{q})\overline{A}_{ij}(\mathbf{q}) = \sum_{\mathbf{k} \in \mathcal{K}} \left( -k_i (q_i - k_i) + \frac{k_i q_i q_j (q_j - k_j)}{\mathbf{q}^2} \right) \overline{h}(\mathbf{k}) \overline{h}(\mathbf{q} - \mathbf{k})$$

$$= \sum_{\mathbf{k} \in \mathcal{K}} \frac{\mathbf{k}^2 \mathbf{q}^2 - (\mathbf{k} \cdot \mathbf{q})^2}{\mathbf{q}^2} \overline{h}(\mathbf{k}) \overline{h}(\mathbf{q} - \mathbf{k}) = \sum_{\mathbf{k} \in \mathcal{K}} |\mathbf{k}|^2 (\sin \theta_{\mathbf{q}, \mathbf{k}})^2 \overline{h}(\mathbf{k}) \overline{h}(\mathbf{q} - \mathbf{k})$$
(C.14)

where  $\theta_{q,k}$  is the angle between the vectors q and k. The magnitude of the above expressions in each mode is then:

$$|P_{ij}^{T}(\mathbf{q})\overline{A}_{ij}(\mathbf{q})|^{2} = \left(P_{ij}^{T}(\mathbf{q})\overline{A}_{ij}(\mathbf{q})\right) \times \left(P_{ij}^{T}(-\mathbf{q})\overline{A}_{ij}(-\mathbf{q})\right)$$

$$= \sum_{\mathbf{k},\mathbf{k}'\in\mathcal{K}} |\mathbf{k}|^{2} (\sin\theta_{\mathbf{q},\mathbf{k}})^{2} |\mathbf{k}'|^{2} (\sin\theta_{-\mathbf{q},\mathbf{k}'})^{2} \overline{h}(\mathbf{k}) \overline{h}(\mathbf{q} - \mathbf{k}) \overline{h}(\mathbf{k}') \overline{h}(-\mathbf{q} - \mathbf{k}')$$
(C.15)

Now, we proceed to calculate the ensemble average of the expression in Eq. (C.15). We emphasize that the averaging is carried out with respect to the trial elastic energy which is presented in Eq. (C.6). We then obtain:

$$\sum_{\mathbf{q} \in \mathcal{K}} \langle |P_{ij}^{T}(\mathbf{q})A_{ij}(\mathbf{q})|^{2} \rangle_{U_{\text{trial}}}$$

$$= \sum_{\mathbf{q}, \mathbf{k}, \mathbf{k}' \in \mathcal{K}} |\mathbf{k}|^{2} (\sin \theta_{\mathbf{q}, \mathbf{k}})^{2} |\mathbf{k}'|^{2} (\sin \theta_{-\mathbf{q}, \mathbf{k}'})^{2} \langle \overline{h}(\mathbf{k}) \overline{h}(\mathbf{q} - \mathbf{k}) \overline{h}(\mathbf{k}') \overline{h}(-\mathbf{q} - \mathbf{k}') \rangle_{U_{\text{trial}}}$$
(C.16)

From Wick's theorem (Kleinert, 2009), the above average—with respect to the *quadratic* trial energy (C.6)—is nonzero only when the modes  $k_i$  are decoupled and that is:

$$\begin{split} \langle \overline{h}(\mathbf{k}_{1})\overline{h}(\mathbf{k}_{2})\overline{h}(\mathbf{k}_{3})\overline{h}(\mathbf{k}_{4})\rangle_{U_{\mathrm{trial}}} &= \langle |\overline{h}(\mathbf{k}_{1})|^{2}\rangle_{U_{\mathrm{trial}}}\langle |\overline{h}(\mathbf{k}_{2})|^{2}\rangle_{U_{\mathrm{trial}}} \left\{ \delta(\mathbf{k}_{1}, -\mathbf{k}_{3})\delta(\mathbf{k}_{2}, -\mathbf{k}_{4}) \right. \\ &+ \left. \delta(\mathbf{k}_{1}, -\mathbf{k}_{4})\delta(\mathbf{k}_{2}, -\mathbf{k}_{3}) \right\} \\ &+ \left. \langle |\overline{h}(\mathbf{k}_{1})|^{2}\rangle_{U_{\mathrm{trial}}}\langle |\overline{h}(\mathbf{k}_{3})|^{2}\rangle_{U_{\mathrm{trial}}}\delta(\mathbf{k}_{1}, -\mathbf{k}_{2})\delta(\mathbf{k}_{3}, -\mathbf{k}_{4}) \end{split} \tag{C.17}$$

Note that the case k = -q + k is true only in zeroth mode when  $q \to 0$ . The only nonzero case for all modes is when k = -k'. Hence, the summation in (C.16) can be obtained as:

$$\begin{split} \sum_{\mathbf{q} \in \mathcal{K}} \langle |P_{ij}^{T}(\mathbf{q}) \overline{A}_{ij}(\mathbf{q})|^{2} \rangle_{U_{\text{trial}}} &= \sum_{\mathbf{q}, \mathbf{k} \in \mathcal{K}} |\mathbf{k}|^{4} (\sin \theta_{\mathbf{q}, \mathbf{k}})^{4} \langle |\overline{h}(\mathbf{k})|^{2} \rangle_{U_{\text{trial}}} \langle |\overline{h}(\mathbf{q} - \mathbf{k})|^{2} \rangle_{U_{\text{trial}}} \\ &= \sum_{\mathbf{q}, \mathbf{k} \in \mathcal{K}} \frac{(k_{B}T)^{2} |\mathbf{k}|^{4} (\sin \theta_{\mathbf{q}, \mathbf{k}})^{4}}{(\kappa^{\text{eff}}(\mathbf{k}) |\mathbf{k}|^{4} + \gamma_{d}) (\kappa^{\text{eff}}(\mathbf{k} - \mathbf{q}) |\mathbf{k} - \mathbf{q}|^{4} + \gamma_{d})} \end{split}$$
(C.18)

Using the above expression in the first order of free energy expansion in (23) will result in the variational free energy that is given in Eq. (26).

#### Appendix D. Parameter selection for repulsive potential

Consider the MD simulation model shown in Fig. D.6, which is similar to the model used for graphene (Fig. 3), by replacing graphene with 100 Ar gas atoms. The lateral dimension of the simulation box is 20 nm by 20 nm. A 6–12 LJ potential is used to describe the interactions between Ar atoms

$$E = 4\epsilon_{Ar} \left[ \left( \frac{\sigma_{Ar}}{r} \right)^{12} - \left( \frac{\sigma_{Ar}}{r} \right)^{6} \right] \quad r < r_{c}$$
 (D.1)

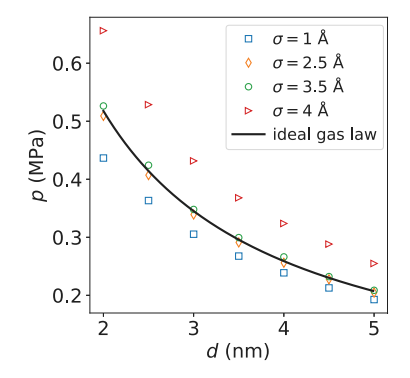
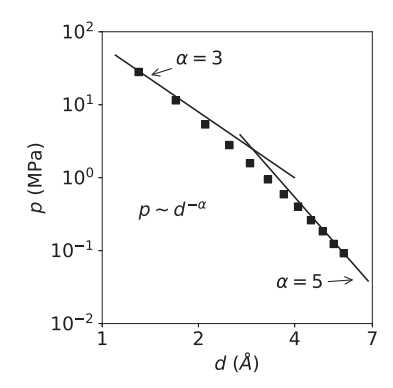


Fig. D.7. Pressure exerted by the walls as a function of the separate distance, d, for different values of  $\sigma$  with a constant  $\epsilon = 1$  eV.



**Fig. D.8.** Steric pressure as a function of wall distance for  $\sigma = 4$  Å.

where  $\epsilon_{Ar} = 0.0104$  eV,  $\sigma_{Ar} = 3.4$  Å and  $r_c = 10$  Å.

The interaction between Ar atoms and the container walls is governed by the repulsive parameters  $\sigma$  and  $\epsilon$ , as defined in the potential given by Eq. (43). Fig. D.7 shows the wall pressure (p) from MD simulations as a function of the separation distance (d), calculated for different  $\sigma$  with a constant  $\epsilon$  at 1 eV. The MD results are compared to the pressure predicted by the ideal gas law. The agreement is achieved when  $\sigma$  is set between 2.5 Å and 3.5 Å. Therefore, it is concluded that  $\sigma = 2.5$  Å can be used to mimic the elastic collision between the wall and confining atoms, which will be adopted for the study of the steric repulsion of graphene.

Finally, we checked the behavior of the scaling law at a different  $\sigma$  value. The p-d curve for  $\sigma=4$  Å is shown in Fig. D.8, which demonstrates that while the pressure values slightly increase due to stronger reaction forces from the walls, the scaling law remains unchanged. Therefore, we postulate that the scaling law remains consistent irrespective of the value of  $\sigma$  as long as the atoms can be effectively confined into the free fluctuation zone with minimum escaping probability.

#### References

Abbena, E., Salamon, S., Gray, A., 2006. Modern Differential Geometry of Curves and Surfaces with Mathematica. CRC Press.

Ahmadpoor, F., Liu, L., Sharma, P., 2015. Thermal fluctuations and the minimum electrical field that can be detected by a biological membrane. J. Mech. Phys. Solids 78, 110–122.

Ahmadpoor, F., Sharma, P., 2016. A perspective on the statistical mechanics of 2d materials. Extreme Mech. Lett.

Ahmadpoor, F., Sharma, P., 2016b. Thermal fluctuations of vesicles and nonlinear curvature elasticity—implications for size-dependent renormalized bending rigidity and vesicle size distribution. Soft Matter 12 (9), 2523–2536.

Ahmadpoor, F., Wang, P., Huang, R., Sharma, P., 2017. Thermal fluctuations and effective bending stiffness of elastic thin sheets and graphene: A nonlinear analysis. J. Mech. Phys. Solids 107, 294–319.

Ahmadpoor, F., Zou, G., Gao, H., 2019. A universal law for interaction of 2d materials with cellular membranes. In: APS March Meeting Abstracts, Volume 2019. pp. V63–015.

Ahmadpoor, F., Zou, G., Gao, H., 2022. Entropic interactions of 2d materials with cellular membranes: Parallel versus perpendicular approaching modes. Mech. Mater. 174, 104414.

Auth, T., Safran, S., Gov, N.S., 2007. Fluctuations of coupled fluid and solid membranes with application to red blood cells. Phys. Rev. E 76 (5), 051910.

Bachmann, M., Kleinert, H., Pelster, A., 2001. Fluctuation pressure of a stack of membranes. Phys. Rev. E 63 (5), 051709. Chen, W., Evans, E.A., McEver, R.P., Zhu, C., 2008. Monitoring receptor–ligand interactions between surfaces by thermal fluctuations. Biophys. J. 94 (2), 694–701.

Chen, D., Kulkarni, Y., 2013. Elucidating the kinetics of twin boundaries from thermal fluctuations. MRS Commun. 3 (4), 241-244.

Chen, D., Kulkarni, Y., 2015. Entropic interaction between fluctuating twin boundaries. J. Mech. Phys. Solids 84, 59-71.

Chen, D., Kulkarni, Y., 2017. Thermal fluctuations as a computational microscope for studying crystalline interfaces: A mechanistic perspective. J. Appl. Mech. 84 (12), 121001.

Dearnley, M., Chu, T., Zhang, Y., Looker, O., Huang, C., Klonis, N., Yeoman, J., Kenny, S., Arora, M., Osborne, J.M., et al., 2016. Reversible host cell remodeling underpins deformability changes in malaria parasite sexual blood stages. Proc. Natl. Acad. Sci. 113 (17), 4800–4805.

Farago, O., Santangelo, C.D., 2005. Pore formation in fluctuating membranes. J. Chem. Phys. 122 (4), 044901.

Fisher, L., 1993. Force between biological surfaces. J. Chem. Soc. Faraday Trans. 89 (15), 2567-2582.

Freund, L., 2013. Entropic pressure between biomembranes in a periodic stack due to thermal fluctuations. Proc. Natl. Acad. Sci. 110 (6), 2047-2051.

Gao, W., Huang, R., 2014. Thermomechanics of monolayer graphene: Rippling, thermal expansion and elasticity. J. Mech. Phys. Solids 66, 42-58.

Gao, H., Shi, W., Freund, L.B., 2005. Mechanics of receptor-mediated endocytosis. Proc. Natl. Acad. Sci. 102 (27), 9469-9474.

Gov, N., Zilman, A., Safran, S., 2003. Cytoskeleton confinement and tension of red blood cell membranes. Phys. Rev. Lett. 90 (22), 228101.

Hanlumyuang, Y., Liu, L., Sharma, P., 2014. Revisiting the entropic force between fluctuating biological membranes. J. Mech. Phys. Solids 63, 179-186.

Helfrich, W., 1978. Steric interaction of fluid membranes in multilayer systems. Z. Nat.forsch. A 33 (3), 305-315.

Helfrich, W., 1986. Size distributions of vesicles: the role of the effective rigidity of membranes. J. Physique 47 (2), 321-329.

Huang, C., Quinn, D., Sadovsky, Y., Suresh, S., Hsia, K.J., 2017. Formation and size distribution of self-assembled vesicles. Proc. Natl. Acad. Sci. 114 (11), 2910–2915.

Kittel, C., 2004. Elementary Statistical Physics. Courier Corporation.

Kleinert, H., 1999. Fluctuation pressure of membrane between walls. Phys. Lett. A 257 (5), 269-274.

Kleinert, H., 2009. Path Integrals in Quantum Mechanics, Statistics, Polymer Physics, and Financial Markets. World Scientific.

Kulkarni, Y., 2023, Fluctuations of active membranes with nonlinear curvature elasticity. J. Mech. Phys. Solids 173, 105240.

Kusters, R., Simon, C., Dos Santos, R.L., Caorsi, V., Wu, S., Joanny, J.-F., Sens, P., Sykes, C., 2019. Actin shells control buckling and wrinkling of biomembranes. Soft Matter 15 (47), 9647–9653.

Lasic, D.D., 1994. Sterically stabilized vesicles. Angew. Chem. Int. Ed. Engl. 33 (17), 1685-1698.

Lee, J.-H., Choi, S.-M., Doe, C., Faraone, A., Pincus, P.A., Kline, S.R., 2010. Thermal fluctuation and elasticity of lipid vesicles interacting with pore-forming peptides. Phys. Rev. Lett. 105 (3), 038101.

Liang, X., Purohit, P.K., 2018. A method to compute elastic and entropic interactions of membrane inclusions. Extreme Mech. Lett. 18, 29-35.

Lipowsky, R., Leibler, S., 1986. Unbinding transitions of interacting membranes. Phys. Rev. Lett. 56 (23), 2541.

Lipowsky, R., Seifert, U., 1991. Adhesion of vesicles and membranes. Mol. Cryst. Liq. Cryst. 202 (1), 17-25.

Mozaffari, K., Ahmadpoor, F., Sharma, P., 2021. Flexoelectricity and the entropic force between fluctuating fluid membranes. Math. Mech. Solids 26 (12), 1760–1778.

Nelson, D., Peliti, L., 1987. Fluctuations in membranes with crystalline and hexatic order. J. Phys. 48 (7), 1085-1092.

Nelson, D., Piran, T., Weinberg, S., 2004. Statistical Mechanics of Membranes and Surfaces. World Scientific.

Noguchi, H., Gompper, G., 2005. Shape transitions of fluid vesicles and red blood cells in capillary flows. Proc. Natl. Acad. Sci. 102 (40), 14159-14164.

Sharma, P., 2013. Entropic force between membranes reexamined. Proc. Natl. Acad. Sci. 110 (6), 1976-1977.

Wang, P., Gao, W., Huang, R., 2016. Entropic effects of thermal rippling on van der waals interactions between monolayer graphene and a rigid substrate. J. Appl. Phys. 119 (7).

Weikl, T.R., Lipowsky, R., 2004. Pattern formation during t-cell adhesion. Biophys. J. 87 (6), 3665-3678.

Zelisko, M., Ahmadpoor, F., Gao, H., Sharma, P., 2017. Determining the gaussian modulus and edge properties of 2d materials: From graphene to lipid bilayers. Phys. Rev. Lett. 119 (6), 068002.

Zhong-Can, O.-Y., Helfrich, W., 1989. Bending energy of vesicle membranes: General expressions for the first, second, and third variation of the shape energy and applications to spheres and cylinders. Phys. Rev. A 39 (10), 5280.

Zhu, F., Leng, J., Jiang, J.-W., Chang, T., Zhang, T., Gao, H., 2022. Thermal-fluctuation gradient induced tangential entropic forces in layered two-dimensional materials. J. Mech. Phys. Solids 163, 104871.